GEOTHERMAL SALT INTRUSION INTO MESILLA BASIN AQUIFERS AND THE RIO GRANDE, DONA ANA COUNTY, NEW MEXICO, USA

BY

LAWRENCE RAY BOTHERN, B.A., B.S., M.A.

A thesis submitted to the Graduate School

in partial fulfillment of the requirements

for the degree

Master of Science

Major Subject: Geology

Minor Subject: Soil Science

New Mexico State University

Las Cruces, New Mexico

December 2003

"Geothermal Salt Intrusion into Mesilla Basin Aquifers and the Rio Grande, Dona Ana County, New Mexico, USA," a thesis prepared by Lawrence Ray Bothern in partial fulfillment of the requirements for the degree, Master of Science, has been approved and accepted by the following:

Linda Lacey
Dean of the Graduate School

Nancy J. McMillan
Chair of the Examining Committee

Date

Committee in charge:

Dr. Nancy J. McMillan, Chair

Dr. Thomas Giordano

Dr. April L. Ulery

Mr. James C. Witcher, MS

ACKNOWLEGEMENTS

I would like to thank the Interstate Stream Commission of the State Engineers Office for funding this research in its entirety. Also the Southwest Technology Development Institute for their support, particularly Jim Witcher for including me in this project and sharing his vast knowledge of geohydrology and geothermal systems. Thanks to the New Mexico Water Research Institute especially John Kennedy, Mike Cleary and Sean Carrasco for their GIS expertise and their help in preparing maps. Fred Phillips and Suzanne Mills at Tech for generously sharing their Rio Grande sample results. Marta Remmenga of the Economics and International Business Department for her help with the cluster analysis. The excellent faculty members who have all gone far beyond expectations in sharing their knowledge, experience, and especially time. Lee who runs the department, none of us could do it without you. JR, Steph, and Risa thanks for your help with the computer, I still hate them. My greatest thanks go to my wife Debbie for many years of continuous support.

VITA

October 6, 1949	Born at Flandreau, South Dakota
1967	Graduated from Flandreau High School, Flandreau, South Dakota
1967-1971	United States Air Force
1979	BS in Biology and BA in Chemistry from New Mexico State University, Las Cruces, New Mexico
1979-1997	United States Air Force
1988	MA in Management from Webster University, Colorado Springs, Colorado
2000-2002	Teaching assistant, Department of Geology, New Mexico State University

Professional and Honorary Societies

Golden Key

New Mexico Geological Society

National Ground Water Association

International Association of Geohydrologists

Publications

Witcher, J.C., King, J.P., Hawley, J.W., Kennedy, J.F., Williams, J., Cleary, M. and Bothern, L., in press, Sources of salinity in the Rio Grande and Mesilla Basin groundwater, WRRI Technical Completion Report 330, New Mexico Water Resources Research Institute, New Mexico State University, Las Cruces, New Mexico

Field of Study

Major field: Geology Geohydrology

ABSTRACT

GEOTHERMAL SALT INTRUSION INTO MESILLA BASIN AQUIFERS AND THE RIO GRANDE, DONA ANA COUNTY, NEW MEXICO, USA

BY

LAWRENCE RAY BOTHERN, B.A., B.S., M.A.

Master of Science

New Mexico State University

Las Cruces, New Mexico, 2003

Dr. Nancy J. McMillan, Chair

During winter low flow periods the Rio Grande delivers unusable brackish water to the city of El Paso, TX. Previously, this brackish water has been considered to result from the concentration of salts in irrigation drainage, as the water is used for agriculture in the Mesilla Valley of New Mexico. Geochemical evidence points to the mixing of geothermal water with shallow ground water that is hydraulically connected to the Rio Grande (Anderholm, 1990; Swanberg, 1975). The purpose of this research is to more fully understand and to quantify the saline contribution from the ground water components to facilitate a more complete water model of the basin.

Thirty-four water samples are collected from wells in the Mesilla Basin that represent a range of basin aquifer waters, as well as the river and known geothermal waters. Waters are tested for pH, temperature, conductance, and alkalinity at the sample site. Samples are analyzed in the laboratory for total dissolved solids, cations, anions, and isotopic ratios of $^{18}O/^{16}O$, $^{2}H/^{1}H$, $^{13}C/^{12}C$, $^{34}S/^{32}S$, $^{87}Sr/^{86}Sr$, and $^{234}U/^{238}U$.

Major and trace ion concentrations indicate that most geothermal and warm wells represent complex mixtures of a geothermal end-member and cold aquifer waters. The large diversity of ion concentrations in basin groundwater results in nearly infinite possibilities of cold end-member water, which in turn leads to results with apparent exceptions to trends. A two end-member mixing model using total dissolved solids and chloride each plotted with sodium, bromide and lithium shows that warm wells average from 18% to 55% of the geothermal end-member water.

Using data of Phillips et al. (2000) for the Rio Grande a three-end-member model is constructed. Rio Grande plots with low chloride (120 mg/L) and high δD (-66 ‰ VSMOW), cold aquifer water is low in both chloride (38 mg/L) and δD (-94 ‰ VSMOW), and the geothermal end-member has high values for both (1620 mg/L and -73 ‰ VSMOW)). The model shows that the saltiest winter river waters

are attained by a 13% contribution of geothermal water mixed with irrigation drainage water in East drain and Montoya drain.

TABLE OF CONTENTS

TABLE OF CONTENTS CONTINUED

LIST OF TABLES

LIST OF FIGURES

INTRODUCTION

The Mesilla Basin provides water for agricultural irrigation, municipal and domestic use to the people who live in Dona Ana County, New Mexico and the City of El Paso, Texas. Irrigated agriculture has provided the basis for economic prosperity in this area that has been occupied since the early 1800s. Irrigation water is provided mainly by surface waters through releases from Elephant Butte and Caballo Dams into the Rio Grande. However, several drought years during the 1950s prompted the drilling of many irrigation wells in the Mesilla Valley. In addition, the shortage of good quality water in the Rio Grande during the non-irrigating months of the year led the City of El Paso to drill several deep wells in the southeastern part of the basin near Canutillo, Texas, to serve their growing municipal needs.

In arid climates, high rates of evapotranspiration concentrate the salts of the irrigation water in the soil. To continue irrigation farming for long periods, excess water must be applied to the fields to leach salts out of the soil. These facts have long been recognized in the Mesilla Valley and resulted in the digging of drainage canals to collect and return the excess water and salt runoff from the irrigated fields to the Rio Grande. During the summer months when irrigation water is being released from the dam, the drainage water mixes with

the water already in the river. Although this raises the salt concentration of the river, the concentration remains at acceptable levels due to dilution. During the winter months, however, the amount of water released from the dams is minimal while the drainage flow from the fields continues as a base flow. Conventional thought is that salts increase in the river to an unusable level (i.e. TDS exceeds 1000 mg/L, Walton et al., 1999) because there is inadequate dilution water available.

There have been several water chemistry studies and models made of the Rio Grande (Leggat et al., 1962; Wilson et al., 1981; Frenzel & Kaehler, 1992; and Nickerson & Myers, 1993). All of these studies have concentrated either on modeling river and irrigation system chemistry or on water production and chemical characterization of the aquifers. To date, however, no study has tried to do a complete salt balance of both surface and ground waters. To do such a salt balance would require an understanding of ground water salt inputs and mixing between aquifers and surface waters.

Impacts by hydrogeologic components to water quality have not been a part of previous models of the basin water system. In order to fully understand the salinity problem, saline additions from these hydrogeologic sources must be understood. Geochemical evidence points to the mixing of geothermal water with shallow ground water

that is hydraulically connected to the river (Anderholm, 1990; Swanberg, 1975). The purpose of this research is to quantify the saline contribution from the ground water components to facilitate a more complete water model of the basin. It will be impossible to solve the Rio Grande salinity problem until we know all components of the salt balance.

In this study, 34 water samples are collected from wells along the Rio Grande that are representative of the waters of basin aquifers, as well as the river and known geothermal waters. Waters are tested for pH, temperature, conductance, and alkalinity at the sample site. Samples are analyzed in the laboratory for total dissolved solids, cations, anions, and isotopic ratios of $^{18}O/^{16}O$, $^{2}H/^{1}H$, $^{13}C/^{12}C$, $^{34}S/^{32}S$, $^{87}Sr/^{86}Sr$, and $^{234}U/^{238}U$. The collected data are analyzed to determine extent of mixing and the salt contribution of geothermal waters to the Rio Grande. The results are used to chemically characterize the waters of different sources and to determine if mixing of distinct water end members is taking place, and if so, to what degree. This approach allows an estimate of how much, if any, salt is added to the waters of the Rio Grande from geothermal sources.

Geologic Setting

The Mesilla Basin is the southernmost of a series of basins along the banks of the Rio Grande as it flows south through New

Mexico. The Mesilla Basin is located mostly in Dona Ana County, New Mexico (Fig. 1), extending from a northern boundary at the Leasburg Dam at the southern end of Selden Canyon, to about 24 km south of the international boarder with Chihuahua, Mexico, a distance of approximately 95 km (Fig. 2). The basin ranges from approximately 8 kilometers wide in the north to 40 km in its central part and covers about 26,000 square kilometers (Witcher et al., in press; and Hawley and Lozinsky, 1992). The Mesilla Basin is bounded on the east by the Dona Ana Mountains, the Dona Ana-Tortugas uplift, Tortugas Mountain, the Franklin Mountains and Juarez Mountains. The Robledo Mountains, the Sleeping Lady Hills, the Aden Hills, the West Potrillo Mountains, and the East Potrillo Mountains border the basin on the west. The Rio Grande flows through the basin roughly from northwest to southeast.

Geology

Mack et al. (1998) provide a detailed summary of southern New Mexico stratigraphy from Precambrian to Holocene. Geologic units exposed in mountain ranges that border the Mesilla Basin also underlie the basin. It will be seen later that two of the oldest formations contribute to the distinct isotopic character of the geothermal end-member water. The older of the two is the Precambrian crystalline basement consisting of granite plutons

Figure 1 Overview map of study area located in Dona Ana County New Mexico.

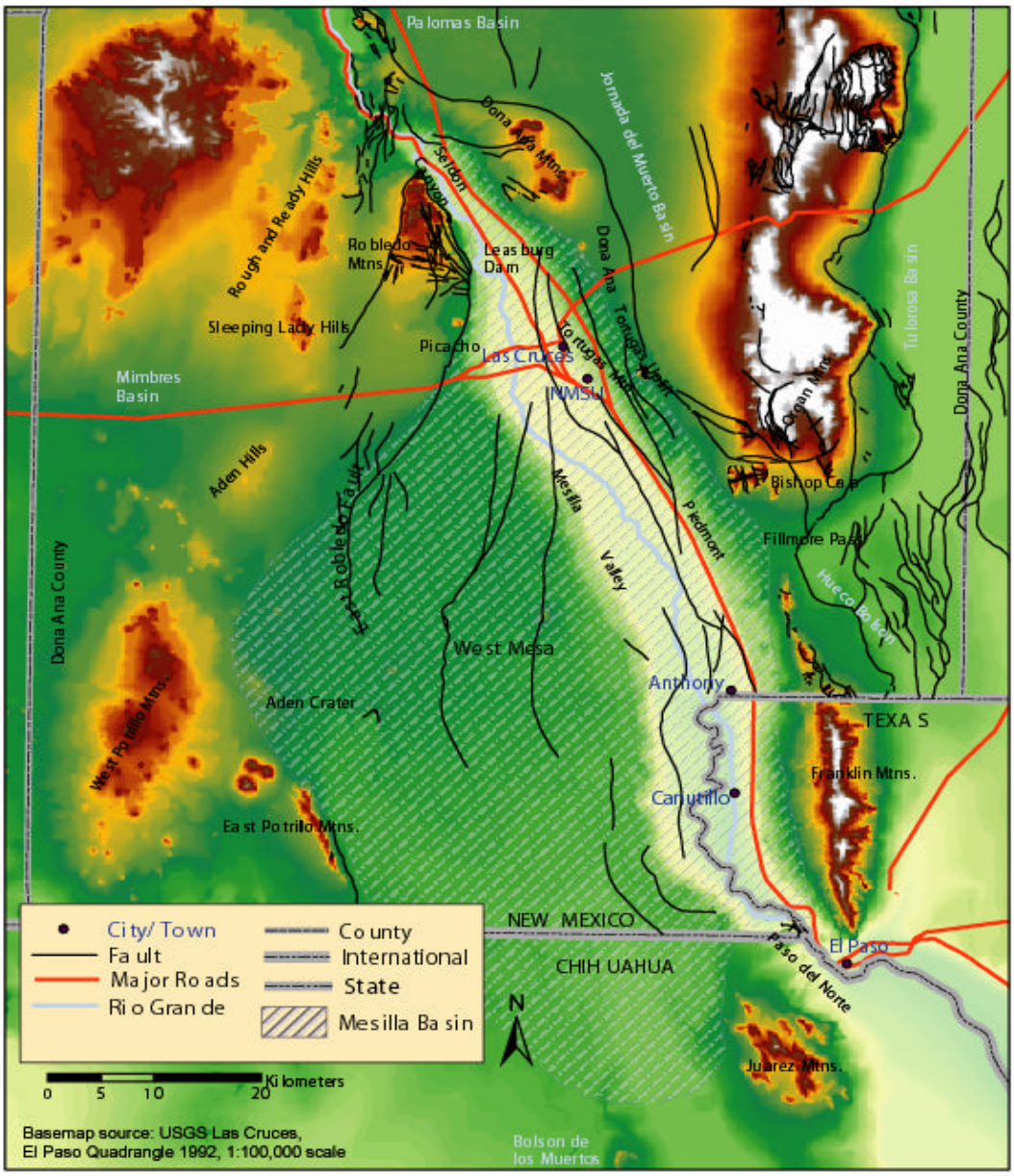

Figure 2 Detail map of Mesilla Basin and surrounding geographic features

intruded into metamorphosed country rock. The younger consists of marine carbonates of Mississippian to Permian age.

The Mesilla Basin sits in a half graben resulting from Rio Grande rifting that began 36 Ma during the Oligocene and is continuing at present (Seager, 1975). Crustal extension or rifting resulted in large crustal blocks tilting to form many grabens and half-grabens, resulting in uplifted mountain ranges and basin subsidence. The entire fill in the Mesilla Basin prior to Rio Grande entrenchment is included in the Santa Fe Group (Hawley and Lozinsky, 1992).

Hawley and Lozinsky (1992) have described the Santa Fe Group in three informal units, as follows:

1. The lower unit is correlative with the Hayner Ranch Formation and the lower Rincon Valley Formations. The lower unit was deposited before the uplift of the current bedrock borders of the basin, between 25 and 10 Ma. Three lower Santa Fe sub-basins existed with a central high point coincident with the current Mesilla Basin. Fine-grained basin floor deposits, intertonguing with alluvial fan deposits underlie distal piedmont slopes from adjacent mountain uplifts in the lower unit. Sandy eolian deposits are interbedded with both the basin floor and piedmont slope deposits. Buried dune complexes up to 150 meters thick are located in the Canutillo area.

2. The middle Santa Fe Group ranges from 10 to 4 Ma in depositional age. During this period tectonism was most active and basin deposition most rapid. Alternating layers of clean sand, silty sand and silt-clay were deposited on broad alluvial flats that terminated in large playa lakes. The sub-basins of the lower Santa Fe were deeply buried during this period. The middle Santa Fe Group probably correlates to the upper Rincon Valley Formation and the lower Fort Hancock Formation (Mack et al., 1998).
3. The upper Santa Fe Group differs significantly from the underlying units, because the bolson environment of an internally draining basin changed to a broad fluvial plain of a through-flowing river. Sandy deposits of this fluvial deltaic system continued to aggrade until about 700 ka. This unit correlates to the Camp Rice Formation that extends throughout central and southern New Mexico and West Texas. In addition to the sandy deposits of the river, this unit also contains local fine-grained facies as a result of channel shifts, and piedmont-slope facies associated with debris-flow deposits. The basal surface interfingers with the middle Santa Fe deposits.

The upper limit of the Santa Fe Group is placed at the surface (La Mesa or West Mesa) of the youngest basin-fill that predates initial

entrenchment of the present Rio Grande valley (Hawley et al., 1969). It is thought that the basin fill is as much as 915 m in some places (Hawley and Lozinsky, 1992, and Nickerson and Myers, 1993). These thickest deposits coincide with the most active segments of major boundary faults (the Mesilla Valley, East Potrillo and East Robledo). However, basin fill is generally between 460 and 760 m in the central basin (Hawley and Lozinsky, 1992).

The upper unit is generally only saturated in the northern third of the basin, and is very permeable due to well-sorted larger grain sizes common in fluvial channels with less cementation. The middle unit is less permeable due to poor sorting of an alluvial fan and greater cementation. The lower unit consists of about 185 m of highly sorted fine eolian sand and is the source of water for El Paso in the Canutillo well field (Hamilton and Maddock, 1993).

During the Pliocene and early Pleistocene about 1.7 to 0.7 Ma, basin deposition stopped and the Rio Grande began to incise into the basin fill of the Santa Fe Group (Mack et al., 1998). This down cutting occurred in irregular cycles separated by partial backfilling and resulted in bench-like surfaces stepping down to the present level of the river. The paired bench-like surfaces are underlain by inset post-Santa Fe deposits of alluvium ranging from about 15 to 40 m in thickness, but generally less than 25 m, in the immediate vicinity of

the river. They consist of well-rounded siliclastic sandy gravels, 6 to 12 m thick, overlain and interfingered with some lenses and layers of sand and clay (Wilson et al., 1981).

The Mesilla Basin may not be hydrologically in complete isolation from adjacent basins. On the north eastern side, for example, a bedrock uplift, designated the Dona Ana – Tortugas uplift (Hawley and Lozinsky, 1992), exists between the Mesilla Basin and the Jornada del Muerto Basin, running from the Dona Ana Mountains southeast, passing near Tortugas Mountain to the southern Organ Mountains. The Jornada del Muerto Basin water generally drains to the northwest and then back to the south with the Palomas Basin drainage, emptying through Seldon Canyon into the Mesilla Basin (Stickel, 1991).

To the east the Mesilla Basin is separated from the Tularosa Basin and Hueco Bolson through Fillmore Pass, the opening between Bishop's Cap at the south end of the Organ Mountains and the north end of the Franklin Mountains. Drilling to a depth of 296 meters in this area has shown that no barrier exists between the two aquifers, and in fact much of the upper portions were deposited simultaneously in both basins because the Rio Grande flowed through the gap at one time (King et al., 1971). The southern extent of the Mesilla Basin is transitional to the Bolson de los Muertos with no bedrock barrier

identified in this region. The East and West Potrillos separate the Mimbres Basin to the west, but several gaps exist. Interbasin flow between all adjoining basins and bolsons with the Mesilla Basin are controlled by the hydraulic properties of fault zones and the adjoining lithologies (Witcher et al., in press).

Both the Rio Grande and the Mesilla Basin empty into Texas through the Paso del Norte. The gradient of the basin floor from north to south is quite small, less than 0.5% (King et al., 1971). The alluvium thins greatly through the narrows and Slichter (1905) measured ground water flow through it at only about 0.1 ft^3/sec. The current flow rate is likely to be higher as a result of pumping drawdown in the El Paso area.

Basin Hydrology

The aquifers in the Mesilla Basin are in both the Santa Fe Group and in the recent flood plain alluvium. Because the Santa Fe Group is of fluvial origin, it is characterized by interfingering of clay layers with coarser sands and gravels; the clays act as discontinuous aquitards. This structure gives the overall result of a leaky confined aquifer. The flood plain alluvium, in contrast, does not have enough thickness or well-defined aquitards to give this result and so it acts as

a shallow unconfined aquifer (Peterson et al., 1984 and Hawley and Lozinsky, 1992).

Hawley and Lozinsky (1992) and Hawley in Witcher et al. (in press) published several cross sections of the Mesilla Basin based on well logs and other geological data. For example, figure 3 shows one of these cross sections in the southern part of the basin, in the vicinity of Anthony, NM/TX. It not only shows the Santa Fe Group divisions, but also shows the more extensive subdivisions of lithoatratigraphic assemblages that describe distribution patterns of major aquifers and confining units.

In discussing the geohydrology of the Mesilla Basin, it is easiest to divide the Basin into three parts: the entrenched Mesilla Valley surrounding the through-flowing Rio Grande, the piedmont slope region east of the Mesilla Valley, and the West Mesa. The Mesilla Valley is the main irrigated agricultural area within the basin, as well as the most populated area. It is impossible to discuss the ground-water hydrology of the Mesilla Valley without also discussing its interaction with surface waters. Irrigated agricultural activity has been occurring in this area since the early 1800s. These activities were at the mercy of a widely meandering stream that frequently flooded the entire valley floor for weeks at a time and in other years or seasons was completely dry. To control the vagaries of the river the

Hydrogeologic Cross Section of the Southern Mesilla Basin

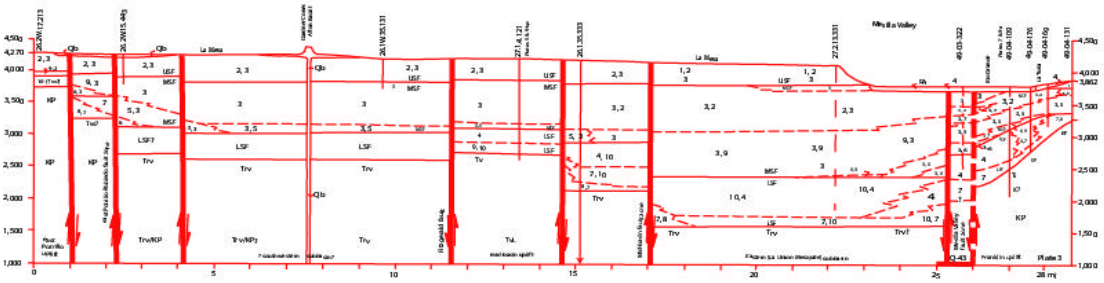

(From Hawley, J., in press)

Figure 3 Cross section of the Southern Mesilla Basin showing Santa Fe Group members and lithostratagraphic assemblages.

U.S. government sponsored the building of Elephant Butte Dam during the early twentieth century (Harris, 1996). This dam, along with the Caballo Dam, is now used to control the water flow in the lower Rio Grande. Within the Mesilla Valley, irrigation water is supplied to the many users through a series of over 75 canals and laterals, while drains are used to collect the excess runoff to keep the water table from rising up to surface level. The river, canals, and flooded fields are hydraulically linked with the ground water of the alluvial aquifer in the Mesilla Valley, providing the majority of recharge in the area.

Wilson et al. (1981) reports that the Rio Grande gains from ground water inflow from Leasburg Dam to a point approximately 6 miles north of Las Cruces. From that point south to the narrows where the river leaves the Mesilla Valley, it contributes water to the underlying aquifers. This has been confirmed more recently by USGS seepage investigations during low flow periods of the river from 1988 to 1998 (Nickerson, 1998). The irrigation canals within the valley are even larger contributors to ground water recharge than the river itself. The flow rates for water recharging the aquifer from these surface water sources are quite variable. Some of this variability is caused by the reduction in permeability of the alluvium making up the channels becoming clogged by clays and fine silt as well as dissolved solids

contained in wastewater effluent. The gradient of saturation below the river and canals also contributes to this variability (Peterson et al., 1984).

Many irrigation wells in the Mesilla Valley were installed to provide ground water during drought years when insufficient water was available from Elephant Butte Dam. Most of these early wells were completed in the flood plain alluvium and the upper portions of the Santa Fe Group. The rapid recharge of these aquifers after several drought years during the mid 1950s further shows the connection of the shallow aquifers to the Rio Grande and the irrigation canals of the valley. Since the 1970s, many more wells were completed entirely in the Santa Fe Group, and since the recharge of these aquifers is from the waters of the flood plain alluvium they are also ultimately recharged mainly from the river system (King et al., 1971; Wilson et al., 1981).

The greatest discharge of ground water from the basin occurs in the Mesilla Valley through pumping for purposes of irrigation (920 wells by 1975, pumping an estimated 110,000 acre-feet per year) and municipal water supplies. The City of Las Cruces has several wells on the east side, along interstate Highway 25. New Mexico State University operates its own wells south of the Las Cruces City wells. Elephant Butte Irrigation District has a well field about five miles

south of the city. Several small towns operate wells further south in the valley, and the City of El Paso operates a major well field north of Canutillo, Texas. Most of these wells are completed in the Santa Fe Group to a depth ranging from 250 to 700 ft (76 to 213 m). The first deep wells (600 to 1,100 ft, 183 to 335 m) in the area were drilled by the City of El Paso in the Canutillo area and were initially reported to be flowing at the surface, although the static surface has dropped since that time due to pumping (Wilson et al., 1981). Hamilton and Maddock (1993) report from various sources that pumping for municipal use in the valley has increased from 6 to 60 cubic feet per day per person (0.17 to 1.7 m^3d^{-1}) from about 1950 to the late 1980s. The three geologic units in the basin contribute to this discharge with varying hydraulic characteristics. Estimated hydraulic conductivity for the upper, middle and lower units are 2 to 68 feet/day (0.61-21m/d), 1-100 feet/day (0.3-335 m/d) and 1-34 ft/day (0.3-10 m/d) respectively. Transmissivities vary from 2,600 to 4,700 $feet^2$/day (242-437 m^2/d), with a storage coefficient of less than 4.3 X 10^{-4} for the middle and lower units (various sources within Hamilton and Maddock, 1993).

In the area east of the Mesilla Valley, aquifer recharge comes from mountain-front and slope-front runoff. The steeper streams empty into flatter, wider, sandy arroyos, which recharge the

underlying aquifers. Runoff in these arroyos rarely reaches the river due to the high permeability of the sands and gravels (Frenzel and Kaehler, 1992).

East of the Mesilla Valley, the Santa Fe Group pinches out quite abruptly against the bedrock high of the Dona Ana-Tortugas uplift that separates the basin from the adjacent Jornada del Muerto basin. Although the alluvium ranges in thickness from 280 to 500 feet (85 to 152 m), the saturated thickness tends to be very thin (Wilson, et al, 1981). Further south in Fillmore Gap, four wells were drilled and show water levels in the Santa Fe Group between 330 and 384 feet (101 and 117 m) below surface level. However, water table contour lines suggest that these wells may be hydrologically part of the Tularosa Basin rather than the Mesilla Basin (King et al., 1971).

The western area of the basin, commonly referred to as the West Mesa, makes up by far the largest area of the basin. Direct rainfall on this large area, however, does not contribute greatly to aquifer recharge due mainly to low precipitation rates and high evaporation rates. Aquifer recharge is further inhibited by caliché and clay layers in the area (King et al., 1971). Aquifer recharge in this area comes mainly from mountain front runoff from the east sides of the East and West Potrillos, and the Robledo Mountains, as well as

the Aden, Sleeping Lady and Rough and Ready Hills (Peterson et al., 1984).

The East Robledo Fault divides the geohydrology of the West Mesa. This fault runs across the mesa in a southwesterly direction from Picacho Peak to Aden Crater. Clays characterize the Santa Fe Group northwest of this fault; only a few wells have been drilled in the area with mostly low production. One well in this area produces over 1,000 gal/min (3.79 m^3/min) (Wilson et al., 1981). Hamilton and Maddock (1993) report that pump tests performed in 1985, by Myers and Orr, show a transmissivity of 5,900 ft^2/day (548 m^2/day) for a well with screened intervals from 710 to 1,210 feet (216 – 369m) below the surface. However, they concluded that this figure was conservative and that transmissivities may be as great as 6,800 ft^2/d (632 m^2/d).

For modeling the Mesilla Basin, Hamilton and Maddock (1993) divide the basin into four layers. Numbered from youngest to oldest, Layer 1 consists of the flood plain alluvium and the uppermost layers of the Santa Fe Group. It is classed as an unconfined aquifer with hydraulic conductivity from less than 20 ft/d (6 m/d) to less than 150 ft/day (46 m/d), and a specific yield of 0.2. Layer 2 is the remainder of the upper Santa Fe Group along with the shallower parts of the middle Santa Fe. It is classified as a confined aquifer that may

become dewatered, with transmissivity ranging from 5,200 to 12,000 ft^2/day (483 – 1115 m^2/d). The storage coefficient is assigned at $4X10^{-4}$. Layer 3, the remainder of the middle Santa Fe Group, is a confined aquifer with transmissivity from 6,000 to 8,400 ft^2/day (557 – 780 m^2/d), and a storage coefficient of $6X10^{-4}$. Layer 4, the deepest aquifer consists of somewhat less area than the upper aquifers. It is characterized as having a transmissivity of less than 6,000 ft^2/day to less than 14,000ft^2/day (557 to 1301 m^2/d) and a maximum storage coefficient of $1.03X10^{-3}$.

SAMPLING

Locations

Thirty-six locations were sampled for analysis (Table 1, Fig. 4). A river sample (MV4) was taken near the entry of the Rio Grande into the Mesilla Valley to represent the waters of the river. It was collected from the Elephant Butte Irrigation District irrigation canal sampling point approximately 100 meters down stream from Leasburg Dam.

Three samples, MV2, 5, and 6, were taken from geothermal production wells. MV2 is the northernmost well sampled on the edge of the basin. It is a composite sample of Masson wells 32 and 33, which are used for space heating of commercial greenhouses. MV5 was taken from New Mexico State University (NMSU) geothermal well PG-1 which is used for space heating of campus buildings, and MV6 (NMSU PG-4) is a geothermal well used for space heating of greenhouses. Both wells are located east of the University campus and west of Tortugas Mountain.

One well (MV25) was sampled in the adjacent Jornada del Muerto Basin and serves only as a reference. The remaining thirty-one samples were collected from wells in the Mesilla Basin. Each sample was numbered sequentially in the order collected, with a general collection trend from north to south. Table 1 shows

SAMPLE #	WELL NAME	SEO NUMBER	LONG	LAT
MV1	Leasburg State Park Well		106.9184	32.4917
MV2	Masson (Composite 32/33)	LRG4489-S-7-8	106.9279	32.5035
MV3	Fort Seldon State Park Well	LRG7710?	106.9213	32.4827
MV4	Rio Grande Leasburg Diversion		106.9214	32.4969
MV5	NMSU PG-1 (geothermal)	LRG520-S(4905)	106.7170	32.2842
MV6	NMSU PG-4 (geothermal)	LRG520-S-3	106.7144	32.2881
MV7	NMSU WELL 14	LRG35-S-4(1851)	106.7618	32.2807
MV8	NMSU WELL 10	LRG35-S-9	106.7534	32.2744
MV9	NMSU HORSEFARM IRRIGATION	LRG1860	106.7763	32.2777
MV10	NMSU HORSEFARM DOMESTIC	LRG1857	106.7752	32.2777
MV11	NMSU FARM NEW WELL	LRG3929-S	106.7426	32.2031
MV12	NMSU FARM OLD WELL	LRG3929-S-2	106.7418	32.1991
MV13	L C WELL 58 (1980 Stern Dr)	LRG430-S-3	106.7798	32.2841
MV14	L C WELL 63 (W Mesa)	LRG430-S-38	106.8721	32.2781
MV15	L C WELL 31 (1901 Isaack Rd)	LRG430-S-18	106.8076	32.3259
MV16	L C WELL 54 (1003 Stagecoach)	LRG430-S-25	106.7517	32.3299
MV17	High Valley Well #21(Bishops Cap)	LRG3918-C	106.5903	32.1441
MV18	JOBE Quarry Well	LRG 7661	106.6371	32.1419
MV19	NM DPS Anthony Port of Entry	LRG8886	106.6075	32.0717
MV20	L C WELL 32 (975 Mesquite)	LRG6430-S-19	106.7508	32.3199
MV21	L C WELL 44 (3994 E.Missouri)	LRG6430-S	106.7467	32.2967
MV22	L C WELL 60 (701 S. Espina)	LRG430-S-35	106.7663	32.3057
MV23	L C WELL 20 (820 Triviz)	LRG430-S-7	106.7509	32.3199
MV24	L C WELL 23 (Hwy 70 & I-25)	LRG430-S-10	106.7688	32.3445
MV25	L C WELL 41 (7990 Holman Rd)	LRG430-S-28	106.6734	32.4172
MV26	MESQUITE WELL ASSN 2	LRG3338	106.6983	32.1640
MV27	MESQUITE WELL ASSN 1	LRG3338-S	106.6982	32.1625
MV28	MESQUITE WELL ASSN 3	LRG3338-S-2	106.6926	32.1652
MV29	MESQUITE WELL ASSN 4	LRG3338	106.6649	32.1399
MV30	CONTRERAS WELL	LRG-8702	106.6899	32.1529
MV31	ANTHONY(NM) WELL 6	LRG4793-S-8	106.6028	32.0189
MV32	ANTHONY(NM) WELL 4	LRG4793-S-3	106.6090	32.0008
MV33	ANTHONY(NM) WELL 1	LRG4793	106.5932	32.0013
MV34	ANTHONY (NM) WELL 3	LRG4793-S-2	106.6031	32.0008
MV35	ANTHONY (TX) WELL 3	TNRCC	106.6096	31.9979
MV36	ANTHONY (TX) WELL 1	TNRCC	106.6064	31.9986

SEO NUMBER is the State Engineer Office tracking number
LONG, LAT are longitude and latitude

Table 1. Sample location and well information

SAMPLE #	TWN	RNG	SEC	QTR	ELEV	DEPTH	prod int
					ft	ft	ft
MV1	21S	1W	11	SWSW	4000		
MV2	21S	1W	10	NWNE		300	200-300
MV3	21S	1W	14	SWNW	3970		
MV4	21S	1W	11	SWNW	3970	surface	
MV5	23S	2E	27	SENENE		860	
MV6	23S	2E	23	NWSWSW		1015	
MV7	23S	2E	29	NESWNE	3882	712	323-463,547-667
MV8	23S	2E	29		3912	766	316-766
MV9	23S	2E	31	NWNENE	3885	154	
MV10	23S	2E	30	SESESE	3885	80	
MV11	24S	2E	20	SENENE		500	
MV12	24S	2E	21	SWSESE		200	
MV13	23S	1E	26		3885	700	
MV14	23S	1W30/2W25?					
MV15	23S	1E	11		3903	617	465-617
MV16	23S	2E	5	SESESE	4190	480	275-479
MV17	25S	3E	12	SENESE		530	471-530
MV18	25S	3E	16	NENWNE		408	241-348, 301-408
MV19	26S	3E	11	SWNWNE		475	400-475
MV20	23S	2E	18			697	456-552,592-696
MV21	23S	2E	21		3994	620	400-600
MV22	23S	2E	18		3940	700	
MV23	23S	2E	16?		4080	680	
MV24	22S	2E	31		4075	596	456-596
MV25	22S	3E	6		4468	1000	
MV26	25S	2E	1	NWNWSW	3835	385	280-380
MV27	25S	2E	1	SWNWNW		260	
MV28	25S	2E	1	NESENW	3835	570	433-553
MV29							
MV30	25S	2E	12	SW,NW,NE		290	280-290
MV31	26S	3E	26	SESWNE	3823	520	300-500
MV32					3825	250	
MV33	26S	3E	35/36		3830	400	
MV34	26S	3E	35	NENWSE	3810	500	280-480
MV35							
MV36							

TWN, RNG, SEC, QTR are township, range, section and quarter of the US Public Land Survey System
ELEV is the elevation of the sample site
DEPTH is the well depth from land surface to water surface, in feet
PROD INT is the production interval or the screened intervals where the well can draw water

Table 1 cont'd

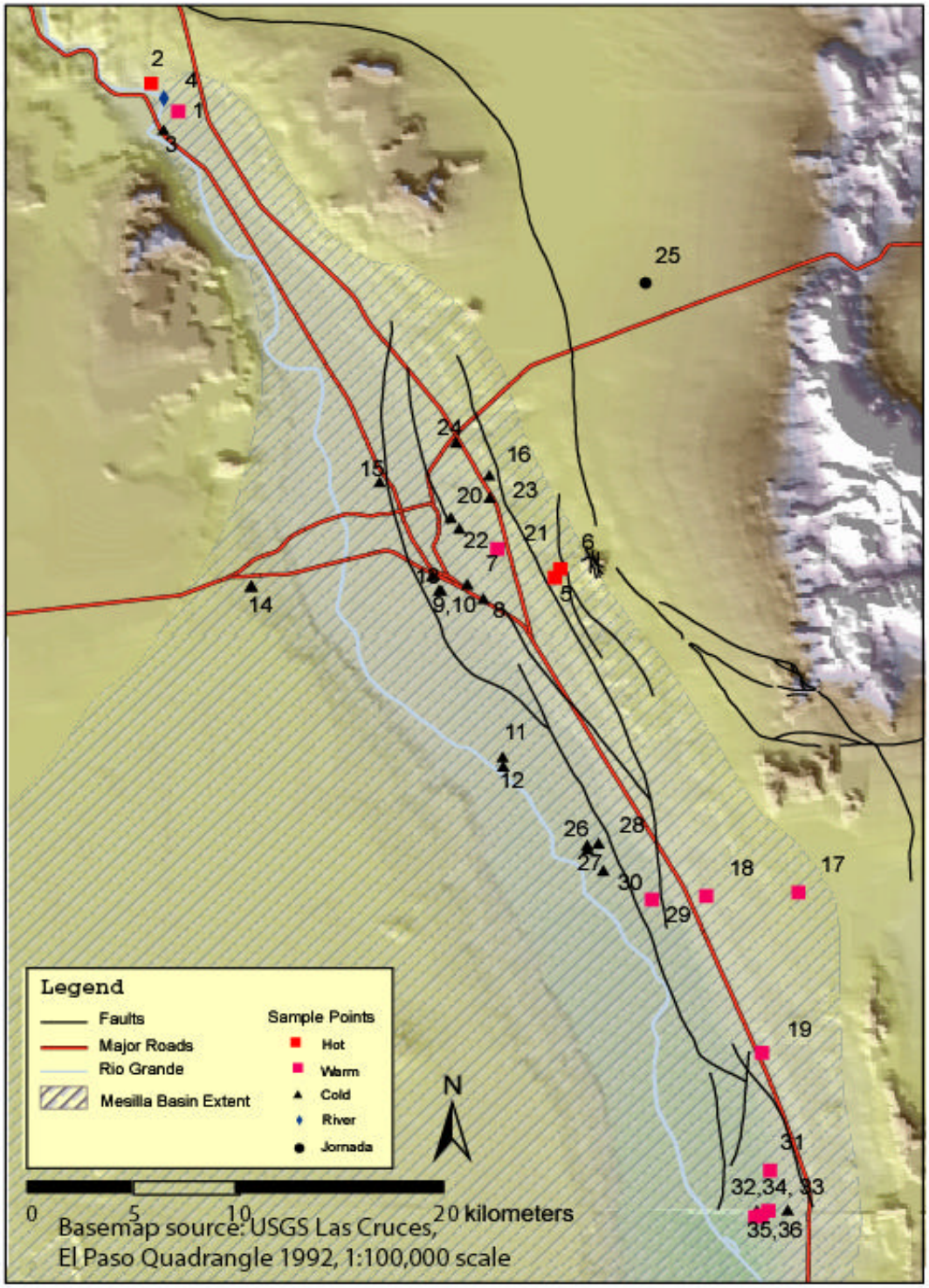

Figure 4 Sample location map

information on well locations, depths, production intervals, pumping rates, and field measurement results.

Procedures

Sampling was accomplished after allowing the installed pump to operate for at least 15 minutes. A 5-gallon (19.2 liter) plastic pail well rinsed with the sample water was used to take a grab sample. Temperature was determined using a digital thermometer. Aliquots were taken for determination of pH with an Oakton pH 10 series meter, and conductivity using an Oakton Con5 Acorn series meter.

Field alkalinity was determined using a Hach digital titrator. A 50 mL sample was pipetted into a beaker with a stirring bar and placed on a magnetic stirrer. A pre-measured packet of Bromcresol Green-Methyl red reagent was added and the solution was titrated with 0.1600 N H_2SO_4 until the color changed to pink. The amount of acid required, as read from the digital counter, times two gives a direct reading of mg/L total alkalinity. Because the pH of all samples is below the dissociation point of $CaCO_3$, all the alkalinity is reported as HCO_3^-.

Eight aliquots of each water sample were collected for laboratory analysis. The $^2H/^{18}O$ sample was collected in amber glass bottles with septum caps, rinsed with sample water. All other samples were collected in high-density polyethylene bottles (HDPE), which were

washed with soap, rinsed once with tap water and rinsed three times with distilled/deionized water (D/DIW). The last rinse was left in the bottles and emptied just prior to sampling. After the preceding wash and rinse, the strontium isotope bottles were placed in a ten percent nitric acid bath for a minimum of 24 hours, followed by three additional rinses with D/DIW. Filtration was accomplished on site with a 45 μm filter and vacuum flask.

The following table shows the amounts and treatments of the samples collected.

SAMPLE	AMOUNT	FILTERED	TREATMENT
$^{2}H/^{18}O$	60 mL	No	None
$d^{13}C$	250 mL	No	Sodium azide
Anions	250 mL	Yes	None
Cations	250 mL	Yes	Acidified to pH < 2 with HCl
$d^{15}N$ Nitrate	1 L	Yes	Acidified to pH < 2 with HCl
$d^{234}U$	1 L	Yes	Acidified to pH < 2 with HNO_3
$d^{34}S$ Sulfate	1 L	Yes	BaCl, $BaSO_4$ precipitate filtered after 6 hr
$^{86}Sr/^{87}Sr$	250 mL	Yes	Acidified to pH< 2 with ultra-pure HNO_3

Table 2 Sample treatment

The results of field and laboratory analyses are contained in Tables 3 and 4. Table 3 shows the field measurements and the laboratory results of the major and trace anions and cations that are used in this analysis and Table 4 shows the isotope analyses, additional laboratory results that are not discussed are presented in Appendix Tables A.1 and A.2. Ion Chromatography was used to measure anion results.

SAMPLE #	TEMP	TEMP	field	lab	field	lab	lab	TDS
	pH	pH	COND	COND	TDS	ion Σ		
	°F	°C			mS/m	mS/m	mg/L	
MV1	79.2	26.2	6.86	7.67	3640	3510	2330	2203
MV2	155.1	68.4	6.72	7.66	6320	5840	3870	3681
MV3	68.2	20.1	7.80	8.02	770	767	510	528
MV4	57.6	14.2	8.32	7.81	756	740	491	547
MV5	137.7	58.7	6.90	7.57	3420	2950	1960	2084
MV6	146.2	63.4	6.59	7.43	3250	2870	1907	2042
MV7	67.9	19.9	7.71	8.13	655	652	435	497
MV8	70.0	21.1	7.69	7.69	546	558	371	431
MV9	66.4	19.1	7.17	7.52	2570	2640	1756	2130
MV10	66.8	19.3	7.92	8.04	467	457	305	356
MV11	67.5	19.7	7.70	7.65	728	732	488	566
MV12	66.2	19.0	7.69	7.67	814	837	558	646
MV13	67.5	19.7	7.92	7.96	533	550	365	439
MV14	76.3	24.6	7.90	7.79	652	646	432	457
MV15	68.4	20.2	7.83	7.83	390	528	351	417
MV16	75.2	24.0	7.56	7.88	924	932	622	685
MV17	85.3	29.6	6.82	7.53	2170	2250	1493	1622
MV18	90.0	32.2	7.10	7.59	2220	2190	1458	1611
MV19	87.7	30.9	7.43	7.94	1945	1947	1294	1335
MV20	71.3	21.8	7.88	7.90	562	581	389	440
MV21	78.8	26.0	7.71	7.64	763	749	497	547
MV22	68.8	20.4	7.38	8.04	1222	1210	810	904
MV23	76.6	24.8	7.37	7.74	1169	1252	832	871
MV24	73.6	23.1	7.40	7.85	1239	1270	846	898
MV25	85.9	29.9	7.64	7.83	508	494	329	437
MV26	68.9	20.5	7.62	7.70	784	774	517	588
MV27	69.3	20.7	7.71	7.86	616	603	401	486
MV28	72.9	22.7	7.82	7.95	544	550	367	440
MV29	92.5	33.6	7.85	8.12	854	836	556	657
MV30	69.1	20.6	7.81	7.76	565	569	379	463
MV31	79.9	26.6	7.48	7.84	2400	2450	1630	1665
MV32	75.8	24.3	7.53	7.82	2300	2350	1560	1506
MV33	76.7	24.8	7.67	7.77	2390	2440	1619	1533
MV34	82.1	27.8	7.80	7.92	1643	1631	1084	1073
MV35	91.2	32.9	8.06	8.03	711	730	485	539
MV36	88.6	31.4	7.91	7.94	1007	898	660	666

TDS mg/L is the laboratory determined TDS

TDS (ion Σ) is the summation of the cations and anions shown in this table, in mg/L

Table 3. Major and trace ion concentration results.

SAMPLE #	Na	K	Ca	Mg	Li	Rb	Sr	Fe
	mg/L	mg/L	mg/L	mg/L	mg/L	mg/L	mg/L	mg/L
MV1	494	48.4	186	25.8	0.311	0.308	2.700	0.421
MV2	1100	149	127	11	0.733	1.230	2.480	0.199
MV3	70.6	36.3	59	8.38	0.105	0.037	1.090	0.081
MV4	91.1	6.35	56.6	11.2	0.066	0.004	0.739	0.081
MV5	470	53.1	162	21	0.315	0.385	4.660	0.214
MV6	452	57.6	168	24.1	0.318	0.396	4.910	0.455
MV7	54.7	4.69	73.8	10.4	0.054	0.024	0.861	0.099
MV8	53.2	5.37	55.1	8.81	0.052	0.027	0.724	0.077
MV9	310	9.07	270	32.2	0.167	0.007	2.820	0.694
MV10	39.2	2.61	51.4	6.52	0.042	0.012	0.541	0.104
MV11	57	3.52	92.9	12.1	0.055	0.004	1.030	0.127
MV12	67.6	4.19	102	12.4	0.058	0.003	1.150	0.142
MV13	61.8	4.66	54.5	8.22	0.074	0.015	0.643	0.118
MV14	49	4.8	69.3	7.54	0.067	0.012	0.917	0.119
MV15	53.5	6.46	55.8	8.48	0.069	0.020	0.621	0.070
MV16	97	8	80.1	16.6	0.077	0.055	1.470	0.109
MV17	299	37.5	150	18.2	0.221	0.248	4.220	0.207
MV18	309	42.7	139	17.5	0.246	0.253	3.840	0.203
MV19	337	20.9	62.4	11.4	0.218	0.091	2.460	0.086
MV20	78.9	7.47	36.3	6.6	0.084	0.030	0.563	0.052
MV21	61.4	5.62	88.4	13.7	0.083	0.030	1.140	0.182
MV22	66.4	9.71	159	26.7	0.076	0.068	2.230	0.345
MV23	87.3	10.1	128	28.5	0.102	0.068	2.400	0.171
MV24	154	6.95	93.2	23.3	0.122	0.041	2.430	0.162
MV25	34.9	2.7	59.4	15.6	0.015	0.004	1.030	0.077
MV26	60.5	22.9	82.3	16.3	0.106	0.008	1.170	0.187
MV27	66.3	15.6	52.8	11	0.115	0.016	0.713	0.175
MV28	69.4	15.2	31.5	7.29	0.114	0.044	0.550	0.103
MV29	144	16.4	26.3	5.58	0.146	0.081	0.744	0.047
MV30	61.5	19.1	47.1	7.43	0.099	0.062	0.814	0.063
MV31	366	32	114	23.5	0.282	0.109	3.990	0.311
MV32	261	49	147	43.1	0.338	0.207	5.210	0.185
MV33	294	41	129	42.2	0.418	0.141	5.140	0.170
MV34	281	10.1	63.3	7.48	0.198	0.044	1.480	0.085
MV35	131	3.8	25.8	0.756	0.095	0.024	0.295	0.043
MV36	163	4.28	43.5	0.911	0.106	0.025	0.448	0.073

Table 3 cont'd.

SAMPLE #	HCO_3	SO_4	Cl	F	Br	B	NO3	SiO_2
	mg/L	mg/L	mg/L	mg/L	mg/L	mg/L	mg/L	mg/L
MV1	245	262	906	0	0.730	0.252	<1.0	31.02
MV2	303	287	1620	4.41	1.200	0.354	<1.0	73.81
MV3	115	65.8	131	0.47	0.147	0.089	<0.02	40.01
MV4	165	139	65	0.62	0.165	0.125	0.06	10.8
MV5	510	228	554	1.09	0.424	0.203	<0.10	78.3
MV6	465	236	578	1.84	0.461	0.218	<0.10	52.84
MV7	170	92.8	63.4	0.39	0.122	0.067	<0.02	25.46
MV8	158	68.8	52.8	0.49	0.105	0.068	<0.01	27.17
MV9	405	806	263	0.36	0.552	0.230	0.33	29.95
MV10	145	47.5	38.1	0.39	0.071	0.062	<0.01	24.6
MV11	183	120	68.9	0.34	0.132	0.073	<0.02	26.74
MV12	195	161	76.4	0.36	0.133	0.077	<0.02	25.67
MV13	170	60.7	50.0	0.54	0.100	0.079	<0.01	27.38
MV14	135	69.7	89.9	0.38	0.136	0.072	<0.02	30.38
MV15	155	55.2	52.3	0.50	0.089	0.075	<0.01	29.09
MV16	175	157	114	0.69	0.327	0.096	0.91	33.59
MV17	528	185	362	0.58	0.313	0.189	0.20	35.94
MV18	508	190	351	1.45	0.311	0.209	<0.10	47.07
MV19	335	169	360	1.39	0.325	0.238	<0.10	34.44
MV20	160	65.2	58.7	0.85	0.099	0.112	<0.01	25.46
MV21	145	96.8	104	0.60	0.232	0.084	<0.02	29.31
MV22	240	212	158	0.25	0.259	0.073	<0.02	28.45
MV23	170	228	184	0.54	0.487	0.092	2.16	29.09
MV24	200	172	209	0.65	0.406	0.171	0.12	35.51
MV25	150	103	13.9	0.61	0.165	0.048	0.83	54.34
MV26	160	111	93.0	1.15	0.173	0.090	0.21	38.94
MV27	175	65.0	55.4	2.00	0.129	0.108	<0.01	42.14
MV28	175	55.9	44.1	1.99	0.083	0.099	<0.01	38.72
MV29	255	97.1	70.4	2.39	0.119	0.113	<0.02	38.29
MV30	178	60.4	46.3	2.14	0.086	0.098	<0.01	40.22
MV31	335	267	485	0.82	0.468	0.231	<0.10	36.58
MV32	193	239	512	0.50	0.910	0.246	3.51	50.7
MV33	175	242	560	0.48	0.982	0.217	0.30	42.36
MV34	185	158	319	0.58	0.319	0.259	2.20	43.86
MV35	128	136	72.7	0.60	0.132	0.232	<0.02	39.79
MV36	113	144	160	0.66	0.177	0.209	<0.02	35.51

Table 3 cont'd.

SAMPLE #	Na	K	Ca	Mg	Li	Rb	Sr	Fe
	mg/L	mg/L	mg/L	mg/L	mg/L	mg/L	mg/L	mg/L
Replicates by Item#:								
Re01		55.30	261	35.20	0.726	0.327	3.770	0.566
Re10	49.8	2.98	50.7	7.94	0.071	0.013	0.535	0.130
Re20	102.0	9.17	33.4	8.91	0.124	0.031	0.612	0.072
Re30	81.1	23.40	46.4	8.62	0.138	0.067	0.822	0.080
Re36		5.50	52.6	1.29	0.125	0.026	0.518	0.101
Found in QA Samples:								
NIST1643d	33	2.86	38.80	11.10	0.034	0.014	0.306	0.196
NIST1643d	21.6	2.38	35.60	7.55	0.016	0.012	0.326	0.139
SLRS4	2.08	0.65	5.92	1.50			0.028	0.110
SLRS4	2.64	0.65	5.73	2.00			0.028	0.115
Expected in QA Samples:								
NIST1643d	22.07	2.36	31.04	7.99	0.017	0.013	0.295	0.091
SLRS4	2.4	0.68	6.20	1.60			0.026	0.103

	HCO_3	SO_4	Cl	F	Br	B	NO3	SiO_2
	mg/L	mg/L	mg/L	mg/L	mg/L	mg/L	mg/L	mg/L
Replicates by Item#:								
Re01					0.869	0.494		
Re10					0.065	0.094		
Re20					0.106	0.141		
Re30					0.088	0.127		
Re36					0.204	0.231		
QA Samples NIST1643d:								
Run 1						0.230		4.14
Run 2						0.128		2.98
Expected						0.145		2.70
Certified value %								
	20	15	3	2.00				3

Table 3 cont'd.

Cation results from ACTLABS Skyline, Tucson, AZ were analyzed byICP-MS except for sodium and potassium, which were by inductively coupled plasma-mass spectrometer (ICP-MS) because of their high concentrations. Oxygen and hydrogen isotope analyses were performed at New Mexico Institute of Mining and Technology, Socorro, NM. Geochron Labs, Cambridge, MA, performed carbon isotope analysis. Strontium isotope analyses were performed at University of Texas at Austin, Austin, TX.

RESULTS AND DISCUSSION

Average river values from Philips et al. (2002) are used for comparison where available. These data consist of an average of 10 river samples taken at 10 km intervals from Leasburg Dam to Anthony, NM for anions, and 2 samples for cations (Leasburg Dam and Hwy 70 bridge in Las Cruces). For these data, the error bars represent ± one standard deviation of the average rather than the full range of the measurements.

Field Measurement Characterization

Results

Several measurements were made in the field, including temperature, pH, electrical conductivity, and bicarbonate alkalinity (Table 3). The bicarbonate value for MV23 was inadvertently not recorded in the field. For all interpretations requiring this number, a calculated value is used. The value was calculated using four geographically nearby wells with similar water chemistry. Temperature and bicarbonate values of these four wells are correlated with a linear correlation coefficient greater than 0.97; thus the formula for the linear trend is used to calculate the bicarbonate value (119.7 mg/L) of MV23 from its temperature. This value was checked by averaging the difference between the field and laboratory bicarbonate values of the four wells then subtracting the average from

the laboratory value of MV23, which gives a value of 118.5 mg/L. The average of the two methods, 119 mg/L, is used in calculations.

Well temperatures (Fig. 5) ranged from a low of 19.0 ^{o}C in MV12 to a high of 63.4 ^{o}C in MV6. The three geothermal production wells' average temperature is 58.1 ^{o}C. The temperature of ten warm wells, MV1, 17, 18, 19, 21, 29, 31, 34, 35 and 36, averaged 29.7 ^{o}C. These warm wells are all considered to have anomalously high temperatures (greater than 26 ^{o}C the mean annual temperature (16 ^{o}C) plus 10 ^{o}C (Witcher, 1981)). All of the hot and warm wells are located in three areas: in the north around Leasburg dam (MV1 and 2), in the central area east of NMSU and southeast Las Cruces (MV5, 6 and 21), and in the south from Anthony north along Interstate Highway 10 (MV17, 18, 19, 31, 34, 35 and 36). The average temperature of the remaining 21 wells is 21.4 ^{o}C. The river sample (MV4) was measured at 14.2 ^{o}C; this sample was taken in March and thus reflects the low atmospheric temperature of the season.

Only one well MV35, has a pH greater than 8 (8.1) (Fig. 6). Five wells have a pH less than 7, those are the three geothermal production wells MV2, 5, and 6 and wells MV1 and 17 with pHs between 6.6 and 6.9. All other wells have pH values between 7 and 8. The Rio Grande sample has high pH relative to the area ground water. River sample MV4 has a pH of 8.3, while the average pH of waters

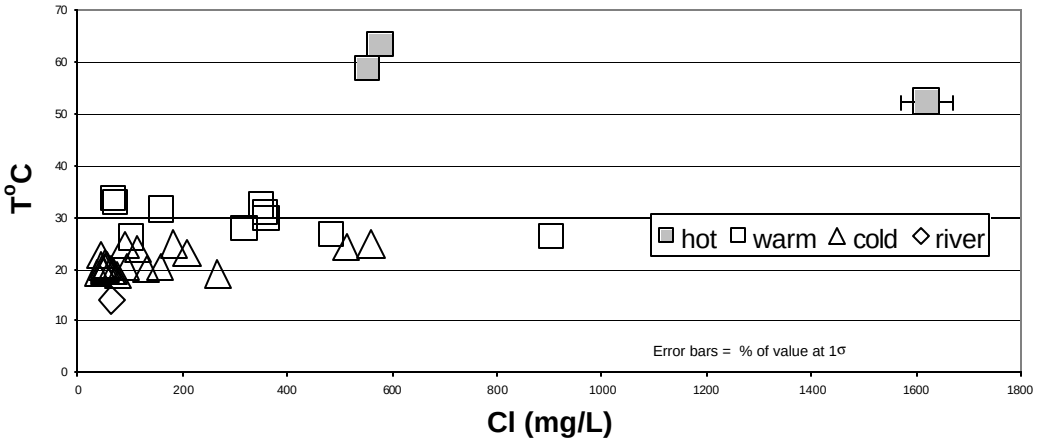

Figure 5 Temperature vs. chloride concentration shows no mixing trend.

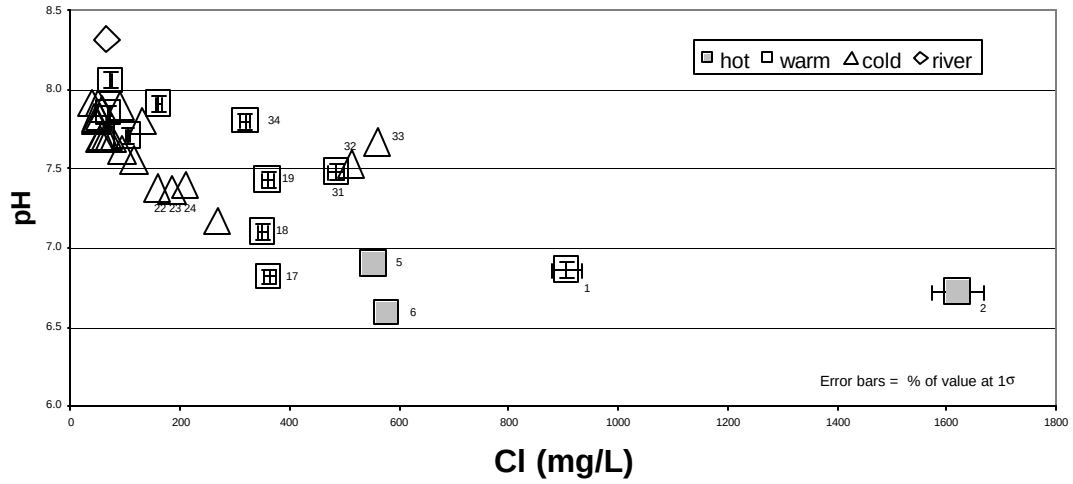

Figurer 6 Field pH vs. chloride concentration shows no linear mixing trend.

from Leasburg Dam to Anthony is 7.9 ranging from 7.54 to 8.29 in summer, and from 8.00 to 8.56 with an average of 8.3 in winter (Philips et al., 2002).

Electrical conductivity (EC) measured in micro-Siemans per centimeter (μS/cm) is the result of the dissolved solids in water being available to conduct current, thus, it is directly related to the total dissolved solids measurement. An EC of 150 to 1500 μS/cm is common in many western US irrigation waters (Sparks, 1995). A plot of EC versus chloride concentration is shown in Figure 7. Well MV2, a geothermal well, has the highest EC and chloride concentration at 6320 μS/cm and 1620 mg/L, respectively. Average EC of the geothermal wells, MV5 and 6, is 2910 μS/cm. Four warm water wells (MV21, 29, 35, and 36) have an EC below 1010 μS/cm while the other warm wells are all above 1640 μS/cm. The cold-water wells generally have EC's below 1240μS/cm with the exception of three wells MV9, 32 and 33, which have an average EC of 2420μS/cm. The lowest conductivity measured is in well MV15 at 390 μS/cm. The river (MV4) was measured at 756 μS/cm with seasonal averages from 930 μS/cm in summer to 1629 μS/cm in winter (Philips et al., 2002). A trend line with correlation coefficient (R^2) of 0.94 has been added for all of the

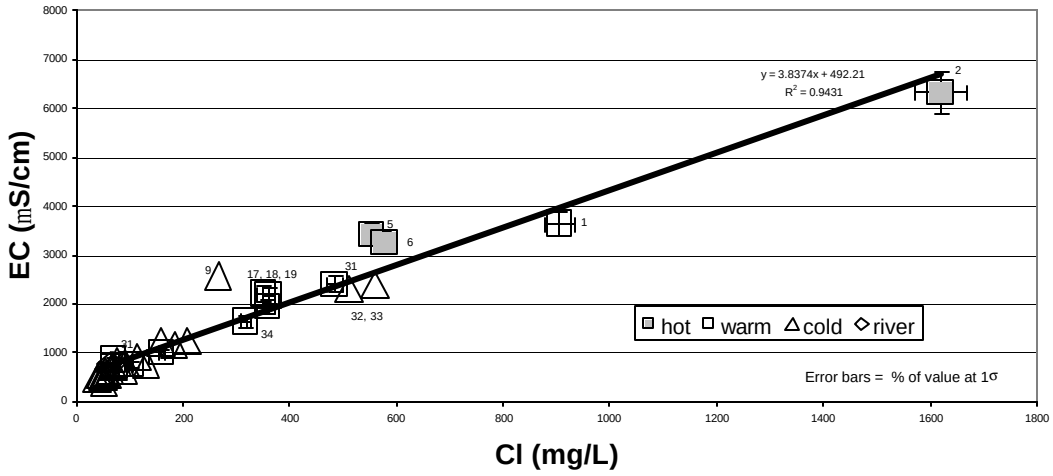

Figure 7 Electrical conductivity vs. chloride concentration shows a linear mixing trend.

wells in this suite. An average multiplier of 0.14 mg/L per µS/cm can be used to convert EC to Cl concentration.

Total dissolved solids (TDS), commonly referred to as salinity, is one of the most common descriptors of water quality. TDS is the summation of all the ions dissolved in the water and is reported here as milligrams per liter (mg/L). TDS was not measured in the field but is discussed here because of its close association with EC. The trend line in Figure 8 for all wells with a correlation coefficient of 0.99 shows the close relationship between EC and TDS. TDS (mg/L) = EC (µS/cm) * 0.67 (mg/L per µS/cm) was determined for this suite of wells, which is very close to the 0.66 (mg/L per µS/cm) value determined by Williams (2001) for the Rio Grande. Fresh water is considered to have a TDS of less than 1000 mg/L, while brackish water has a TDS between 1,000 and 10,000 mg/L. Figure 8 shows that the same twelve wells that had high electrical conductivities also have high total dissolved solids, and fall into the brackish water classification. In addition to the geothermal wells and most of the warm wells, cold wells MV9, 32 and 33 are brackish as is the river average in winter. Warm wells MV21, 29, 35, and 36 all have TDS measurements below 1000 mg/L with an average of 550 mg/L.

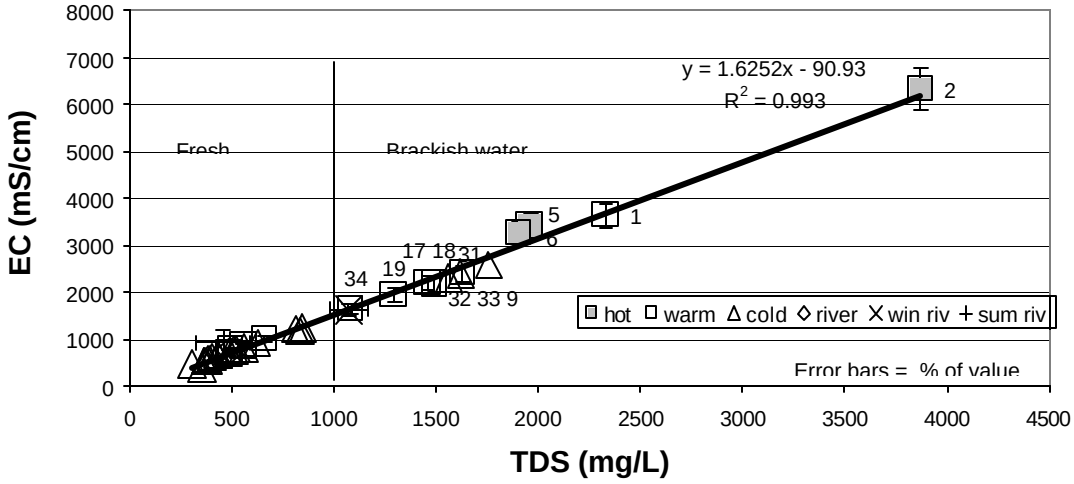

Figure 8 Electrical conductivity (EC) vs. total dissolved solids (TDS) concentration shows a linear mixing trend.

Interpretation

The mixing of two end member waters to form water of intermediate composition is recognizable if two conditions are true: 1) the chemical ions in all of the waters are accurately measured, and 2) the ions do not dissociate or react during mixing to form new molecules. Those ions that do not react and move with mass flow along with water are referred to as conservative. Chloride is one of the most common conservative ion found in water (Hem, 1985). Therefore chloride is used in this study as a basis to compare against other ion measurements. If other ion concentrations plotted against chloride concentration fall along a straight line connecting two end members then the intermediate waters could be mixtures of the two end members. The proportion of each end member contributing to the mixture is represented by the ratio between the mixture and the opposite end member (Hounslow, 1995).

As can be seen in Figure 5 the well temperatures do not fall on mixing lines between end members when plotted against chloride, and thus provide no evidence of mixing between end member waters to form water of intermediate temperature. One explanation for this is conductive heat transfer resulting in some wells like MV1, 32 and 33 having intermediate chemistry but not warm temperatures, and wells like MV21, 29, 35 and 36 without intermediate chemistry but with

intermediate temperatures. Graphs of the pH and bicarbonate (Figs. 6 and 9) against chloride give the appearance that several of the warm wells and a few of the cold wells have intermediate levels that could be the result of mixing between the hot end member MV2 and cold aquifer waters. However, this does not provide convincing evidence of mixing because pH and bicarbonate are not conservative.

The electrical conductivity and total dissolved solids (Figs. 7 and 10) show evidence for mixing between the cold waters of the Mesilla Basin and the geothermal end member to form intermediate warm waters. The mixtures include hot wells MV5 and 6; warm wells MV1, 17, 18, 19, 31, 34; and cold wells MV9, 32 and 33. Warm wells MV21, 29, 35 and 36 plot in the lower left with the cold wells and do not appear to represent mixtures. This is not enough evidence to be convincing that mixing occurs in the Mesilla Basin aquifers. It is much more common in water studies to use the major anions and cations to determine mixing.

Major Ion Characterization

Results

Three major anions and four major cations dominate most natural waters, and have long been used to characterize both surface and ground waters. The major anions are chloride (Cl^-), bicarbonate (HCO_3^-), and sulfate (SO_4^{2-}). The major cations are sodium (Na^+),

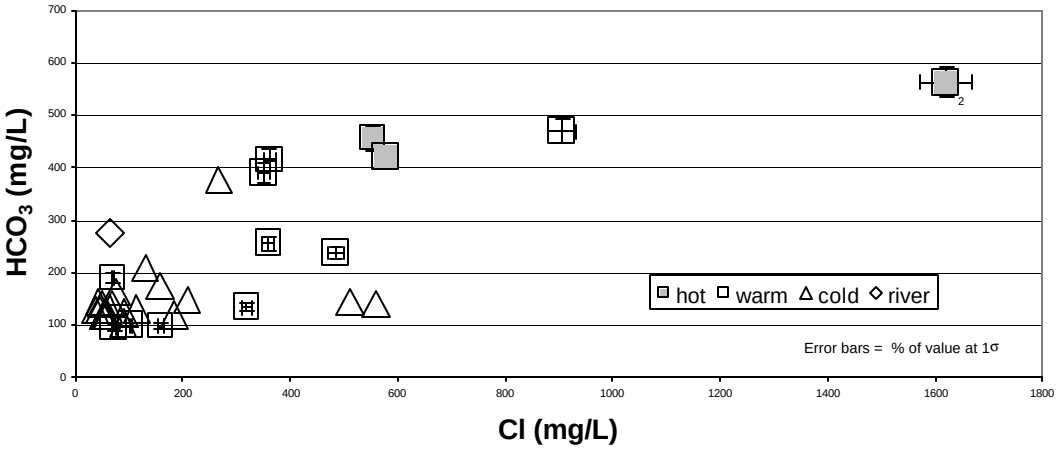

Figure 9 Bicarbonate (HCO_3^-) concentration as a function of chloride concentration shows no linear mixing trend.

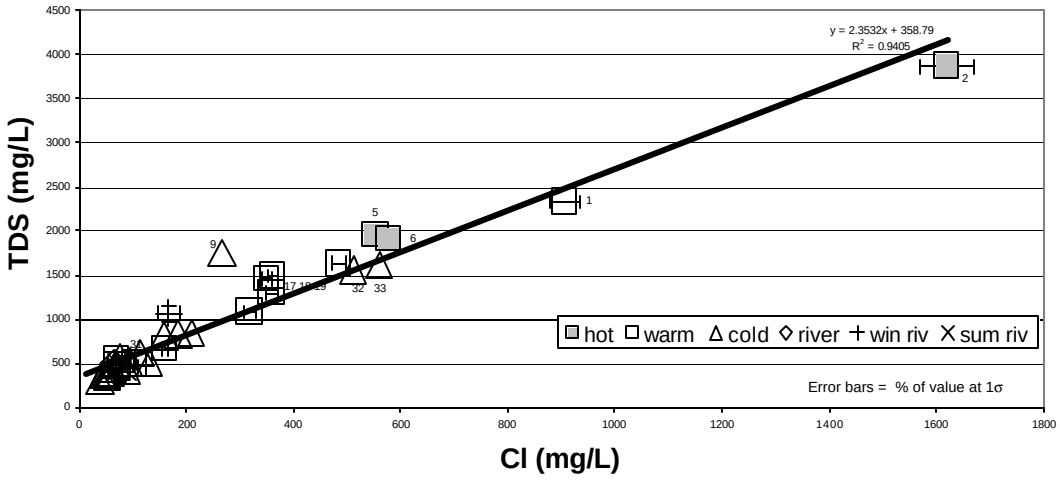

Figure 10 Total dissolved solids (TDS) concentration vs. chloride concentration shows a linear mixing trend.

potassium (K^+), calcium (Ca^{2+}), and magnesium (Mg^{2+}). The concentrations of these ions are shown in Table 3 and Figure 11. The Piper diagram was produced using Rock Ware's Rock Works Toolbox geochemical analysis program. The program recalculates the input data from parts per million (ppm) or milligrams per liter (mg/L) into units of milli-equivalents per liter (meq/L). Equivalents represent moles of positive or negative charges contributed by ions. In the Piper diagram the data are plotted as a percentage of the total meq/L in the anion and cation trilinear diagrams and then projected along straight lines onto the central diamond (Piper, 1944). Because only three cations can be plotted, the sodium and potassium values are added together to form an alkali corner.

In the anion trilinear plot (Fig. 11), most of the points fall within the central inverted triangle with no dominant type. The hot wells and most of the warm wells, however, fall mostly within the chloride corner; three warm wells (MV21, 29, and 35) fall within the central area of no definite type. The cold wells that fall outside the no dominant type area are MV9, a lone point in the sulfate type area, and wells MV32 and 33 in the chloride type. Well MV9 and all of the

chloride type wells have brackish TDS content. The river water plots very close to bicarbonate type but in the no dominant type area.

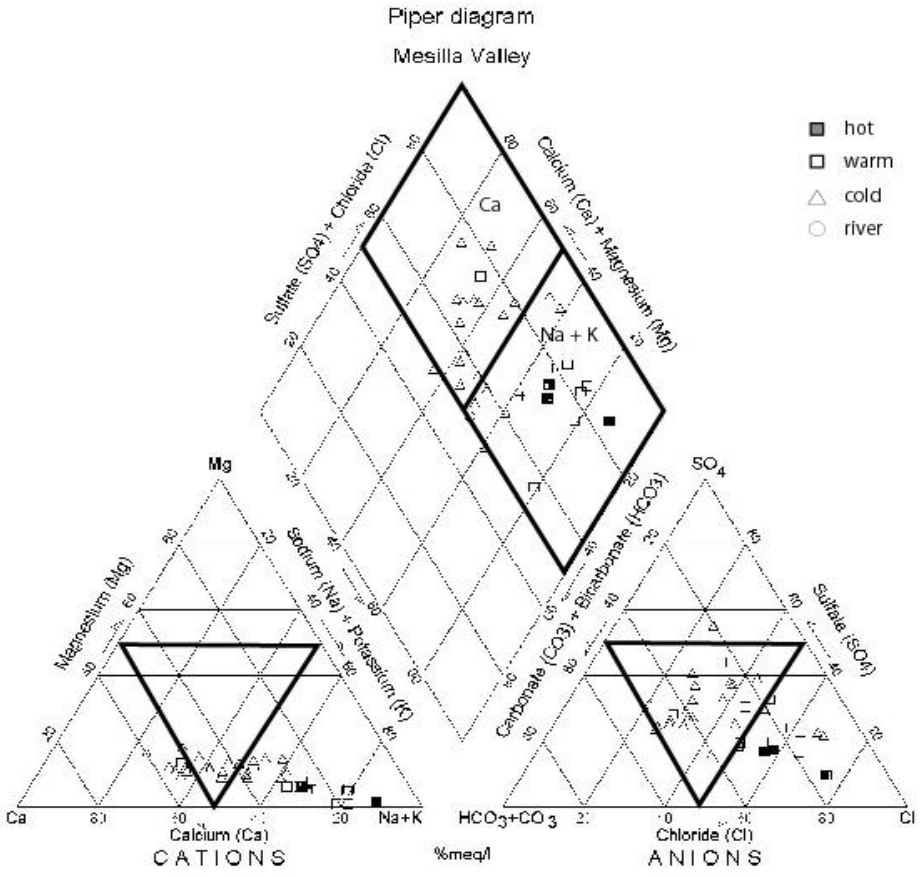

Figure 11 Piper diagram of study wells.

In the cation trilinear plot the Mesilla Basin data stretch in a fairly narrow band from the alkali corner towards the calcium and slightly in the magnesium directions. All points fall within three areas. The hot and warm wells are alkali type with the exception of MV21, which is calcium type. The cold-water wells range from alkali type to calcium type, and the river plots as alkali type.

In the central diamond area of the Piper diagram all of the wells fall into two areas that are predominantly calcium or alkali. The Piper calcium-type contains most of the cold-water wells plus warm well MV21. These waters are characterized as primary calcium and sulfate plus chloride. Piper alkali waters include the river, the hot wells and most of the warm wells plus cold wells MV3, 20, 24, 28, 30, 32 and 33. These waters are characterized as alkalis and chloride plus sulfate. In all of the waters chloride and sulfate dominate over bicarbonate.

Well MV2, the hottest geothermal well, has the highest concentration of all of the major anions in this suite with HCO_3 at 562 mg/L, SO_4 of 287 mg/L, and Cl^- of 1620 mg/L. It plots nearest to the chloride corner of the Piper anion trilinear diagram, about 75% chloride. MV2 is a composite sample from two geothermal wells that are mixed during pumping. Anderholm (1990) sampled one of these wells and based on the high chloride concentration of geothermal

wells he concluded that this water may contain a small component of local ground water but it represents the composition of area geothermal water.

Discussion

Freeze and Cheery (1979), Mazor (1997), Hounslow (1995), Brown (1998) and Guler et al. (2002) reviewed several methods that have been used to analyze major anions and cations in natural ground waters. Three multivariate methods were chosen for the analysis of the Mesilla Basin waters: a Piper diagram (Piper, 1944), finger print diagrams (Mazor, 1997), and hierarchical cluster analysis (Alther, 1979; Williams, 1982; Rosenthal et al., 1990; Guler, et al, 2002), which provide a multivariate statistical approach.

Piper Diagram

In a Piper diagram (Fig. 11), possible water mixtures must fall along straight lines between the end-members in each of the three parts of the Piper diagram; additionally, the proportionality of the mixture must remain the same in all three parts (Piper, 1944). There are only two cases of warm water samples that fall on end member mixing lines in all three parts of the Piper diagram (MV2 + MV23 = MV31 and MV34) (Fig. 12); however, the proportionality is not maintained in the anion trilinear plot for either mixed water. Thus, no warm water wells can be explained by simple mixing of the

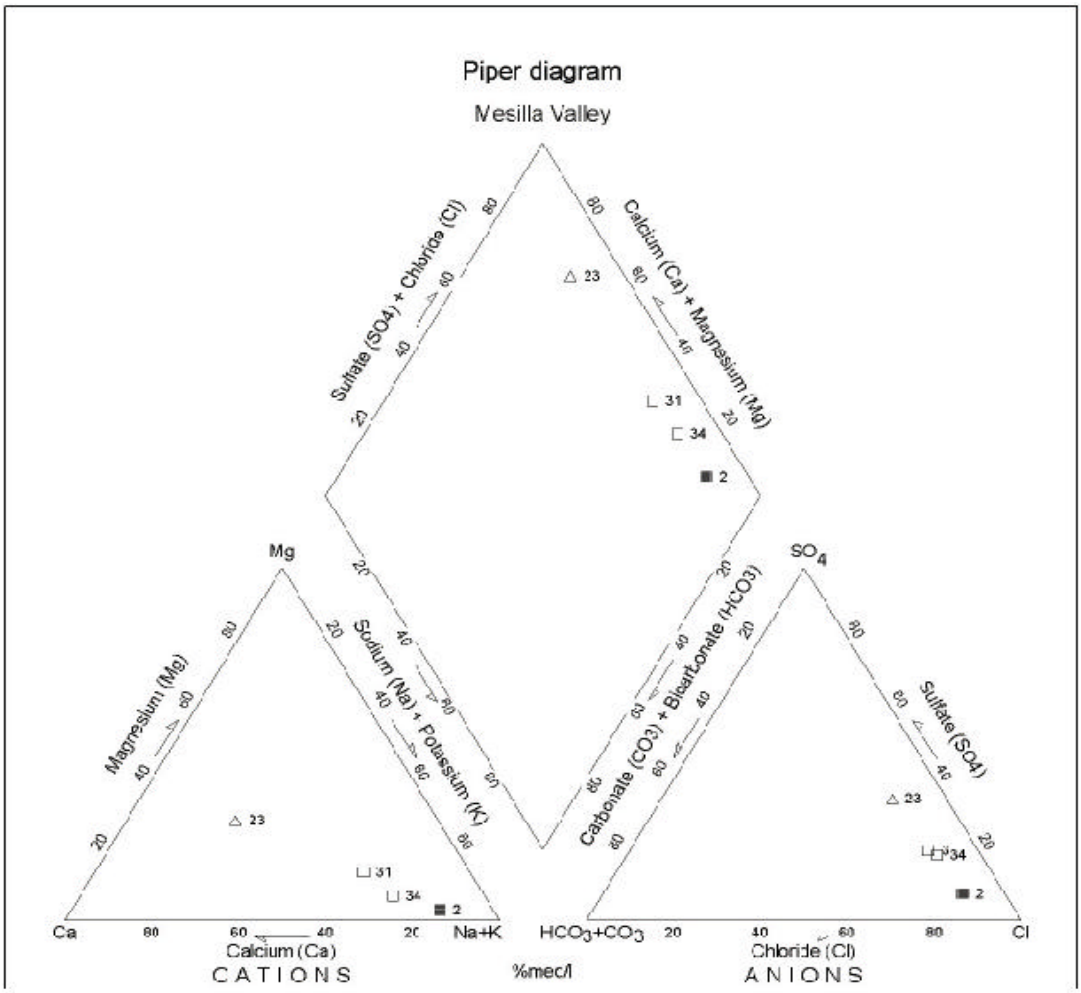

Figure 12 Piper diagram showing possible mixtures of hot and cold end member waters.

geothermal end member with any single sampled cold water well. This does not rule out more complex mixtures of multiple cold-water sources nor mixing with a single unsampled cold-water source, or the modification of the anion levels after mixing occurs. Even though a mixture cannot be confirmed, the Piper diagram still allows similarities and differences of the Mesilla Basin waters to be recognized.

Fingerprint Diagrams

Fingerprint diagrams of the waters are shown in Figures 13 and 14. The diagrams use concentration units of milli-equivalents per liter to achieve results as close as possible to the Piper diagram method. Ion concentrations are plotted on a logarithmic scale in order to plot the wide range of concentrations on a single diagram. In the case of dilution the shape of the fingerprint will remain the same as the saline water but at lower values.

The fingerprint diagrams show that greater variation exists within the anions of both the calcium and alkali type waters than is shown in the Piper diagram. Fingerprints show the Piper calcium waters fall into three groups: with Cl^- as the dominant anion and lesser concentrations of HCO_3^- and SO_4^{-2} including wells MV14, 21, 22, 23 and 26 (Fig. 13a); with HCO_3^- as the dominant anion: wells MV7, 8, 10, 13, and 15; and with SO_4^{-2} as the dominant anion in

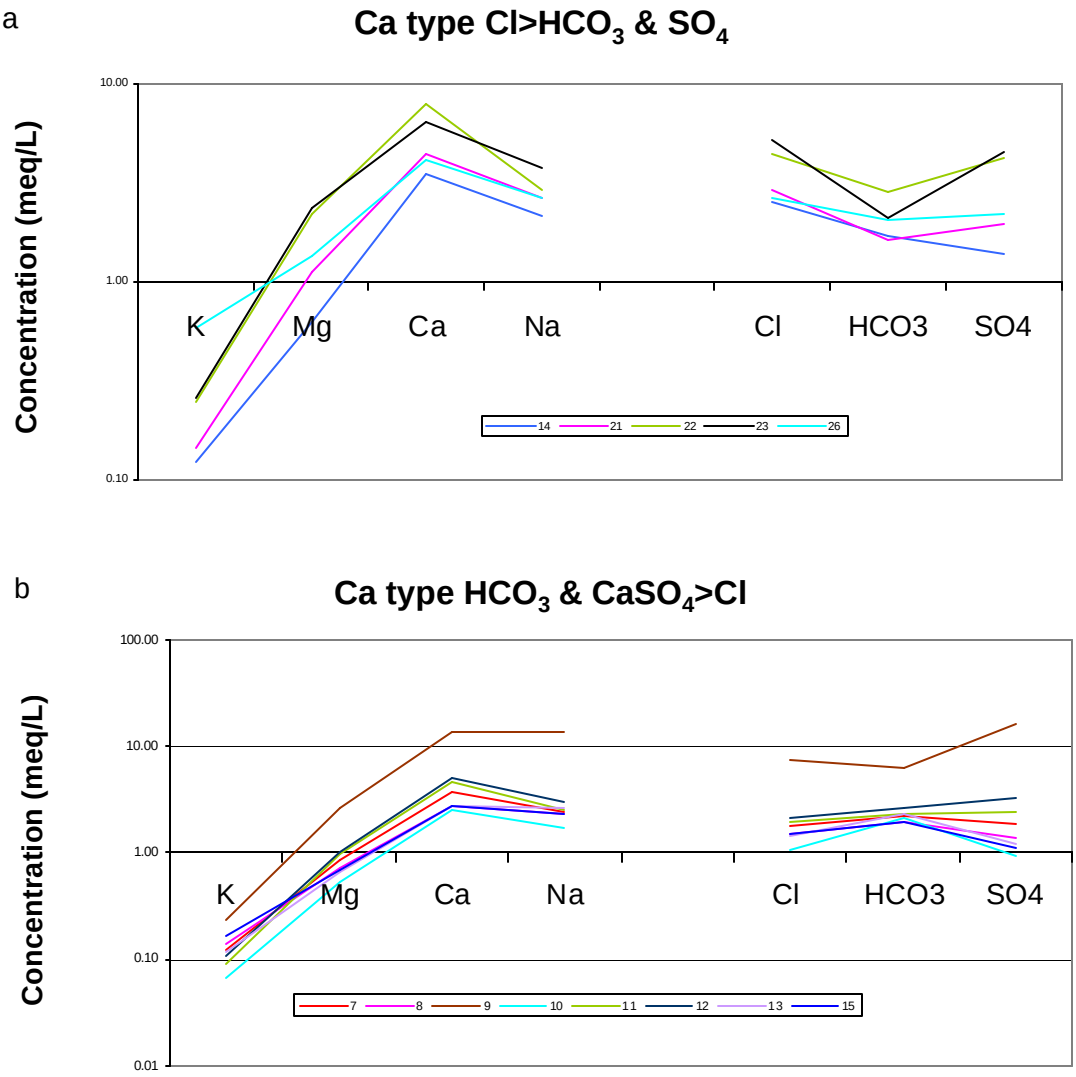

Figure 13 Fingerprint diagrams of calcium type waters.

a

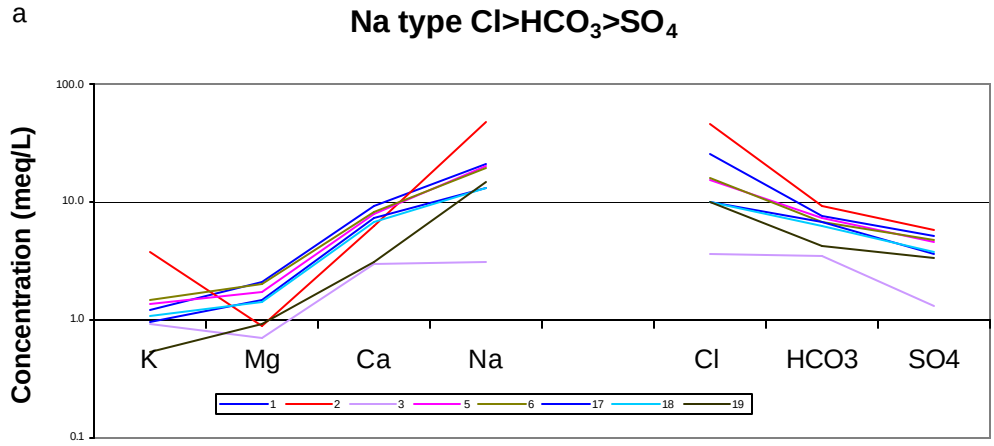

b

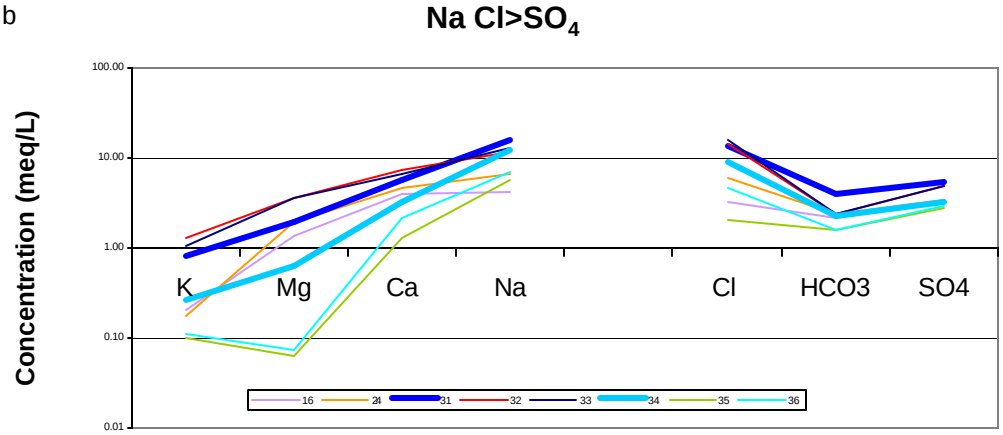

c

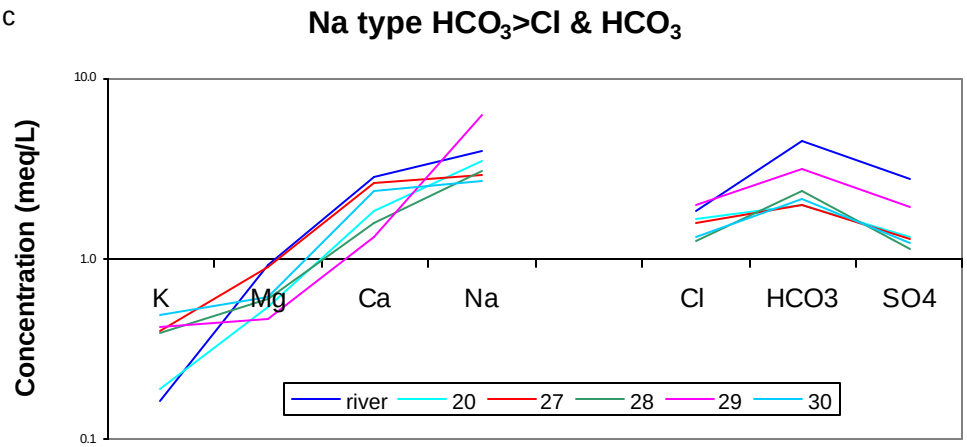

Figure 14 Finger print diagrams of sodium type waters.

wells MV9, 11 and 12(Fig. 13b). The Piper alkali waters also fall into three classes. First are sodium chloride waters, in which bicarbonate exceeds sulfate; these include wells MV1, 2, 3, 5, 6, 17, 18, and 19 (Fig.14a). This group includes many of the hot and warm wells of this suite. Second are sodium chloride waters in which sulfate exceeds bicarbonate, including MV16, 24, 31, 32, 33, 34, 35, and 36 (Fig.14b). The third type of Piper alkali water is sodium bicarbonate water including the river, and wells MV20, 27, 28, 29, and 30 (Fig.14c). MV27, which falls in the Piper calcium water area, proves to be sodium sulfate water when fingerprinted. The reason for this is that the calcium and magnesium are summed during projection into the Piper diamond, but are considered separately in the fingerprint diagram. Similarly, the Piper Diagram shows no bicarbonate waters but the fingerprint diagrams show both calcium and sodium bicarbonate waters. This is a result of the summation of chloride and sulfate being greater than fifty percent in the Piper diagram where it is displayed as a percentage, but when looked at individually bicarbonate is the dominant anion in several wells.

Water fingerprint types result in several geographic groupings shown in Figure 15. Alkali waters tend to be prevalent in the north, south and east while calcium waters prevail in the west central area, roughly from Las Cruces to Mesquite. High sulfate waters are

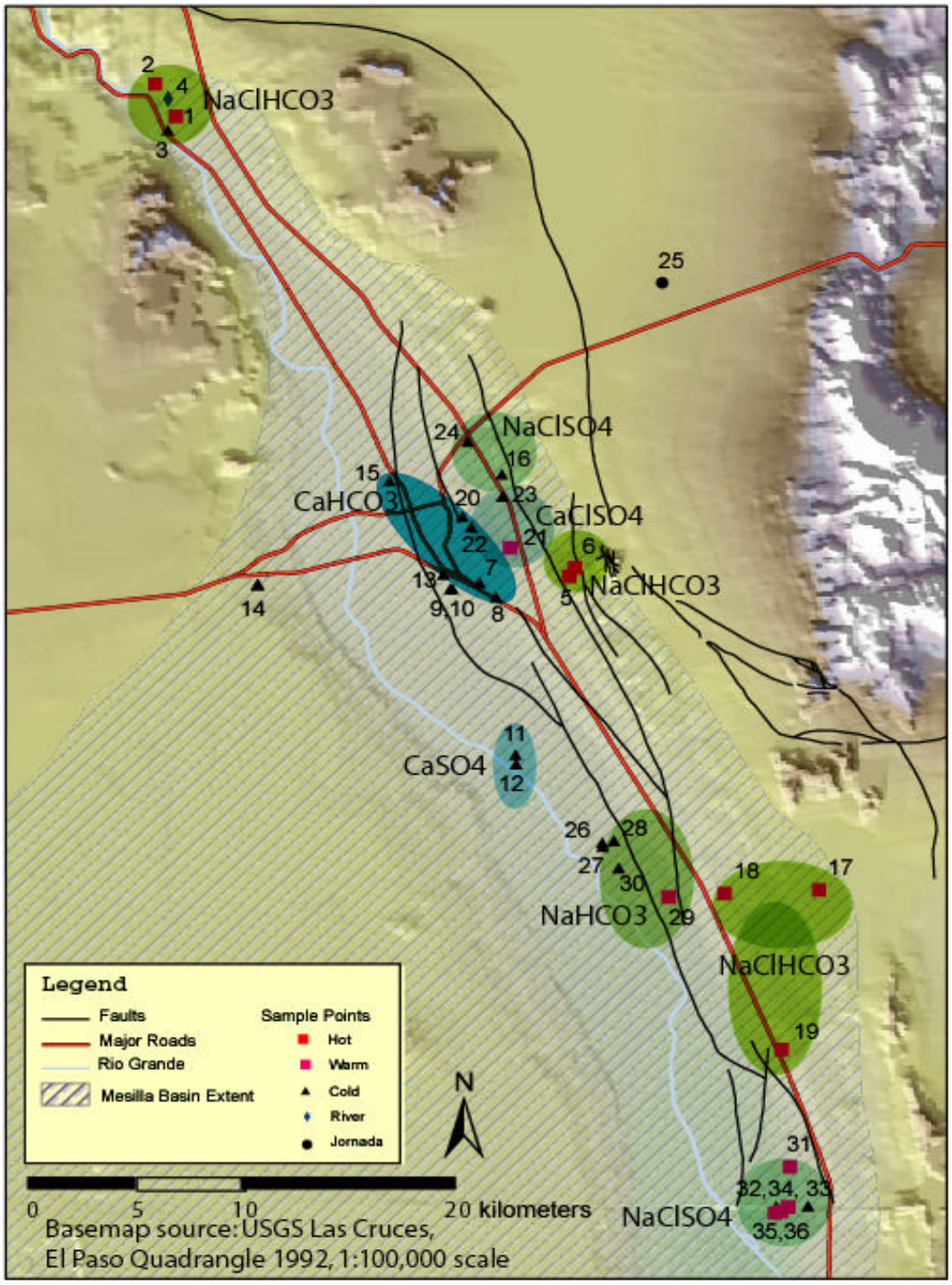

Figure 15 Map showing geographic relation of bicarbonate and sulfate waters .

localized in three areas: a north-south area from MV24 to MV21; another north to south area from well MV9 to MV11 and 12, and all of the wells at the southern end of the suite, including wells MV31 to 36. High bicarbonate waters are found in the Mesquite area with sodium and with calcium in a north south area from MV15 to MV8 in the Las Cruces area. These groupings are an indication that one or more of the ions is in equilibrium with aquifer minerals or that concentrations are related to some other localized phenomena. The high sulfate waters could be the result of gypsum dissolution, for example. This suggests that at least some of the major elements are the result of cold-water reactions that are modifying the chemistry of some warm waters after mixing has occurred. It may also explain why the anions do not maintain strict proportionality in the three mixing examples of the Piper diagram.

Figure 16 shows a fingerprint diagram of the two possible mixtures that were identified in the Piper diagram. Broken lines show the proposed mixed waters while the end members are shown with solid lines. In Figure 16 MV31 appears to be a reasonable fit for a mixture of MV2 and 23, although the magnesium seems a bit high. MV34, in contrast, has higher magnesium than either end member and very low bicarbonate. Keep in mind that these are chemically possible mixtures but the water samples are separated by great

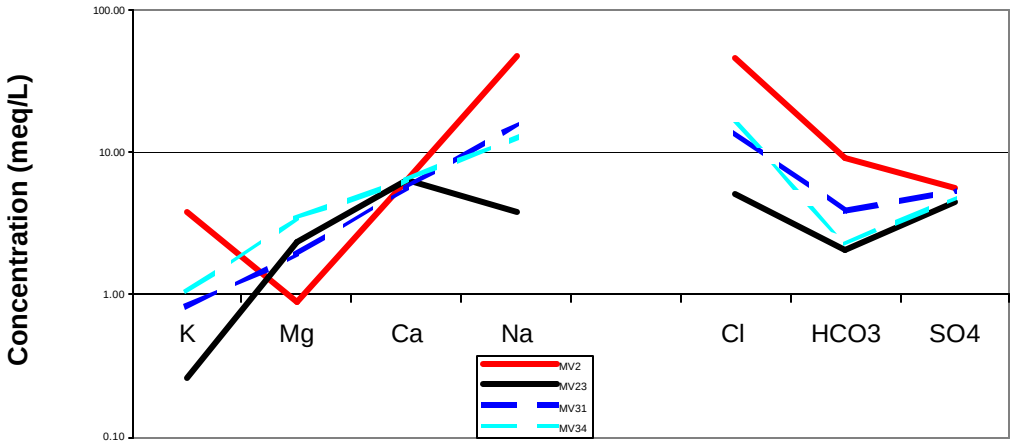

Figure 16 Fingerprint diagram mixed waters shown in Figure 12 Piper diagram

distances. One end member MV2 is from the northern boundary of the basin, the other end member is from Las Cruces, in the center of the basin, and the possibly mixed waters are from Anthony near the southern end of sampled waters. These distances make mixing of the end members to form a mixture unlikely. However, chemically similar waters may appear in multiple locations throughout the basin, and thus end members may be mixtures of unsampled waters that are similar to the samples in this suite.

Hierarchical Cluster Analysis

For hierarchical cluster analysis, the data were converted to meq/L prior to loading into the Statistical Analysis System (SAS) program. This was done to provide results as close as possible to the other methods. In cluster analysis the six concentrations of each well are plotted in six dimensional space by the program. An algorithm calculates the distance between all points, and joins the two nearest points to form a cluster. The next nearest point is then sought and compared to all other points; this point may be added to an existing cluster or it may form a new cluster with its nearest of the remaining points. The process is continued until all points are clustered. Some distant points like MV2 and MV9 result in single point clusters. The objective is to maximize the difference between clusters, while minimizing the difference between points within clusters (Brown,

1998). The results of the cluster analysis are shown as a dendrogram in Figure 17. Considering only the five highest clusters, Mesilla Valley waters have two single well clusters labeled E and D (MV 2 and MV9, respectively). Cluster C is made up of cold wells MV22, 23, 32 and 33; cluster B contains hot and warm wells MV1, 5, 6, 17, 18 and 31; and a large cluster A includes all other wells, including warm wells MV19, 21, 29, 34, 35, and 36.

Fingerprint diagrams of clusters A, B, and C have been plotted in Figure 18. The logarithmic scale has not been used so the full effect of the variations within groups can be seen. Warm wells MV19 and 34 have been added to groups B and C and appear as broken lines in all of these graphs. This change was made to highlight the fact that these two wells appear to fit in either group B or C with as little within-group variation as they appear to exhibit in group A. Group A appears to benefit from averaging a large number of results to produce a smaller within group variation.

Several researchers (Alther, 1979; Ochsenkuhn et al., 1997; Salvania and Nicholson 1990; Veldeman et al., 1990; Williams, 1982) have used cluster analysis to classify waters in the past, but it does not appear suitable for this application. More trials using other ions with the major ions or more major groups may give more useful results.

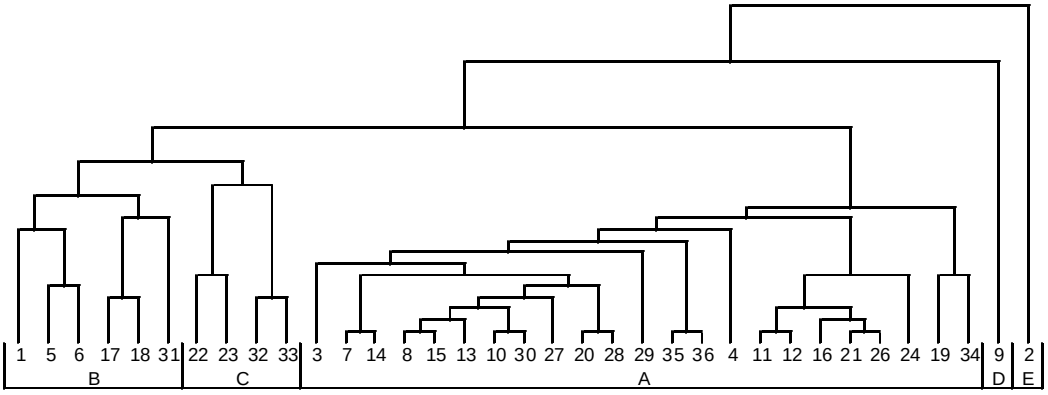

Numbers represent wells, letters represent cluster groups.

Figure 17 Dendrogram of cluster analysis based on variation in six major elements.

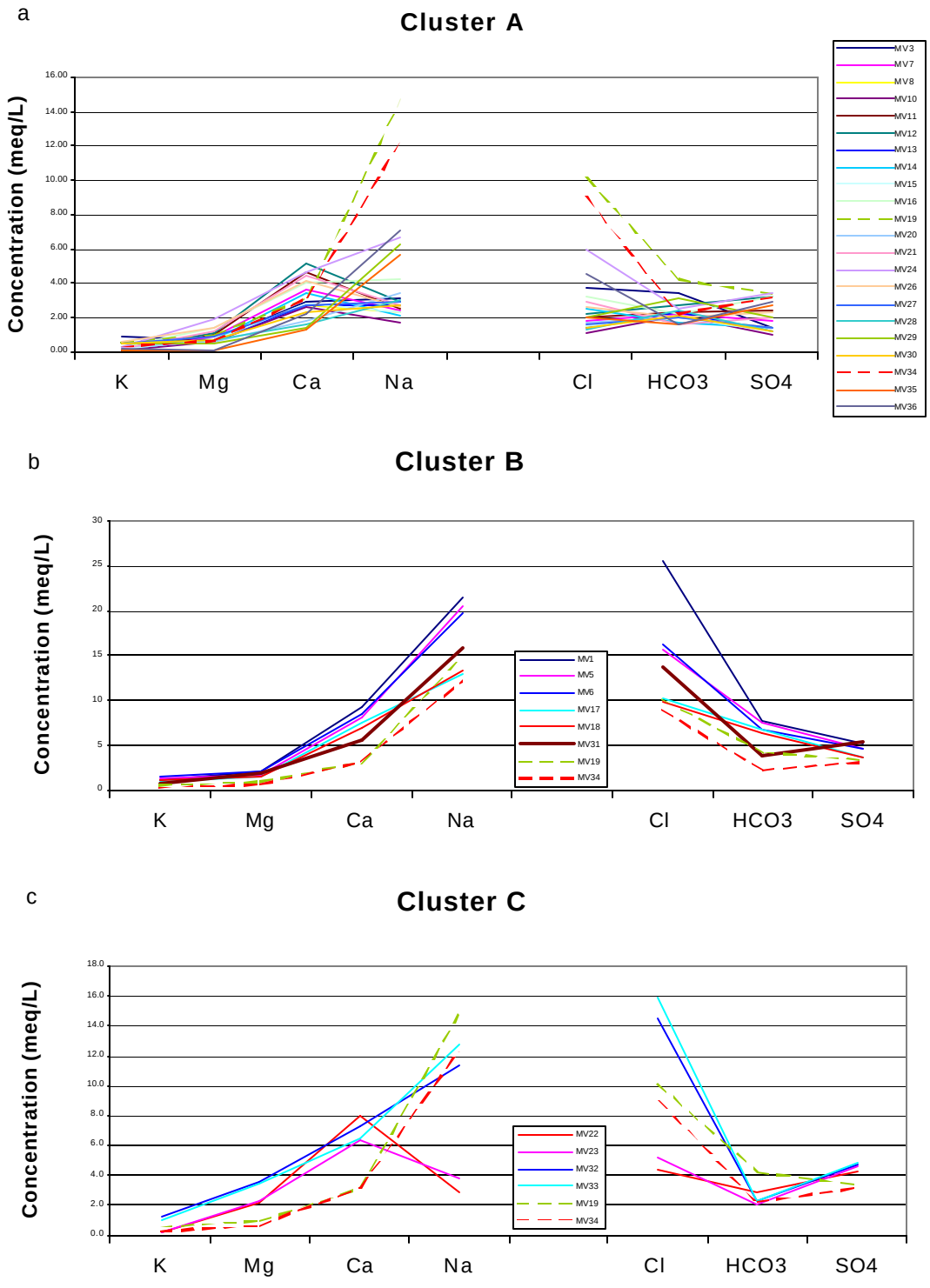

Figure 18 Fingerprint diagrams of clusters.

Summary

In summary, the Piper diagrams give an indication that warm-water wells in the Mesilla Basin could be the result of regional geothermal waters mixing with cold local aquifer waters. Although only one example of mixing is shown, the Piper diagram alkali water types as delineated with the fingerprint diagrams (Fig. 13) give a general indication that the geothermal and most warm wells represent mixed waters. Several cold wells, MV3, 20, 24, 28, 30, 32 and 33, plot with the hot and warm wells as alkali type waters and may be the result of geothermal influence, although too small to have raised their temperatures. The major elements also show that there may be modification of water chemistry by some localized phenomena after mixing has occurred with area geothermal water. Trace elements or ion ratios may further clarify this system.

Ratios and Trace Ions

Results

Bromine

Typically, chloride acts conservatively in ground water; that is, it does not enter into chemical reactions and thus its concentration is only affected by mixing end-member waters. Bromine acts much like chlorine in solution; both exist mainly as the monovalent anions

bromide (Br^-) and chloride (Cl^-). Bromide is considerably less abundant in natural ground waters, but is conservative and even more soluble than chloride, thus the chloride-bromide ratio acts conservatively in most waters (Davis et al., 1997). The chloride – bromide concentrations are shown in Table 3. Bromine concentrations range from a low of 0.089 mg/L at well MV15 to a high of 1.20 mg/L in geothermal well MV2. When the chloride/bromide mass ratios are plotted against chloride, the points fall into two separate groups (Fig.19). The three geothermal production wells, most of the warm wells and cold well MV3 have ratios between 890 and 1350 with an average of 1125. All other wells and the river have ratios below 661 with an average of 525. This group includes three warm wells MV21, 29 and 35. Cold wells MV32 and 33 have surprisingly low Cl/Br ratios for their chloride concentrations.

Lithium and Boron

Lithium and boron are two trace elements that are used extensively in modeling geothermal water, because they are generally conservative and present in only very small amounts in cold water. The concentrations are presented in Table 3. When plotted as a function of chloride concentration (Fig. 20), an apparent mixing line is observed between the cold water with lithium concentrations below 200 μg/L and the geothermal end member at 733μg/L of lithium. The

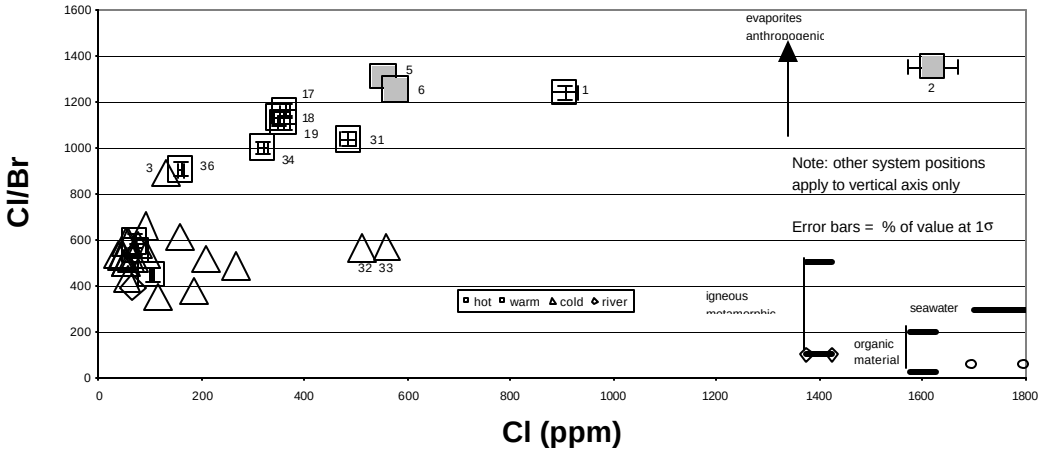

Figure 19 Chloride/bromide ratio vs. chloride concentration

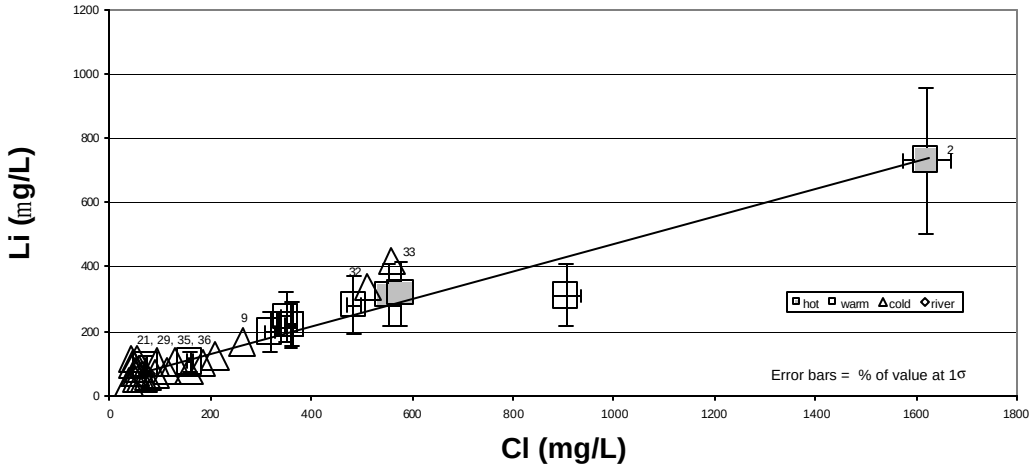

Figure 20 Lithium concentration vs. chloride concentration shows a linear mixing trend.

average lithium concentration in the cold-water wells is 86 μg/L with a standard deviation of 31 μg/L, excluding wells MV32 and 33. In contrast the average concentration for the warm-water group of wells (excluding MV21, 29, 35 and 36, but including hot wells MV5 and 6 and cold wells MV32 and 33) is 286 μg/L with a standard deviation of 67 μg/L.

Figure 21 presents the boron concentrations as a function of chloride; the concentrations are similarly divided into two groups but without the obvious mixing line between the geothermal end member and the cold wells. Most of the cold wells plus warm wells MV21 and 29 are below, and the hot and most warm wells and cold wells MV9, 24, 32 and 33 are above 150 μg/L. The average boron concentration of cold wells is 84 μg/L with a standard deviation of 15μg/L; the warm well group average concentration is 226 μg/L with a standard deviation of 21 μg/L. MV2 has a boron concentration of 354 μg/L.

Silica

Silica as a function of chloride also plots along an apparent mixing line between cold and geothermal end members. However, this appearance may be due more to the chloride distribution than to silica concentrations. The highest silica concentrations (Table 3) of the suite are in the three hot wells, which average 68 mg/L, with a

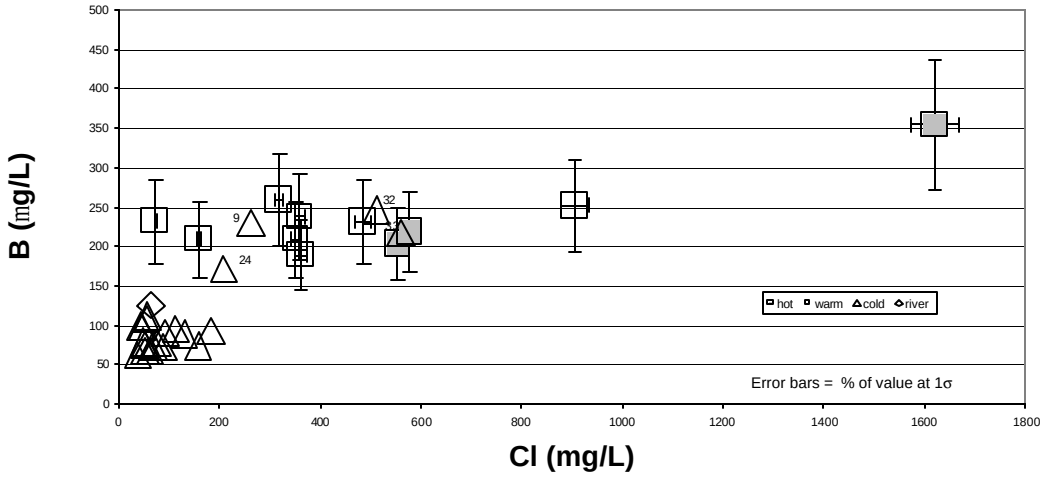

Figure 21 Boron concentration vs. chloride concentration shows no linear mixing trend

standard deviation of 14 mg/L (Fig. 22). There is much less difference between the warm and cold water silica levels. The warm-water average concentration is 40 mg/L with standard deviation of 7 mg/L, while the cold-water average is 32 mg/L with standard deviation of 6 mg/L.

Discussion

Chloride/Bromide Ratio

Bromide, like chloride, is extremely soluble in water and normally does not enter into precipitation or dissolution reactions other than the formation of evaporites. As a result, the chloride/bromide (Cl/Br) mass ratio is conservative in most natural ground waters. This ratio is quite low in most natural systems like seawater (290), meteoric water (50-180), organic materials (20-200), and igneous and metamorphic rocks (100-500) (Davis et al., 1997). Higher mass ratios come mainly from anthropogenic sources (road salt, sewage and others) or the dissolution of evaporite minerals (Fig. 21).

The Cl/Br mass ratio is a dimensionless number calculated from the concentration of ions in units of mg/L. High mass ratios in evaporites are a result of the differential solubility between bromide and chloride. Because bromide is so much more soluble than chloride, halite forms as nearly pure sodium chloride crystal matrix

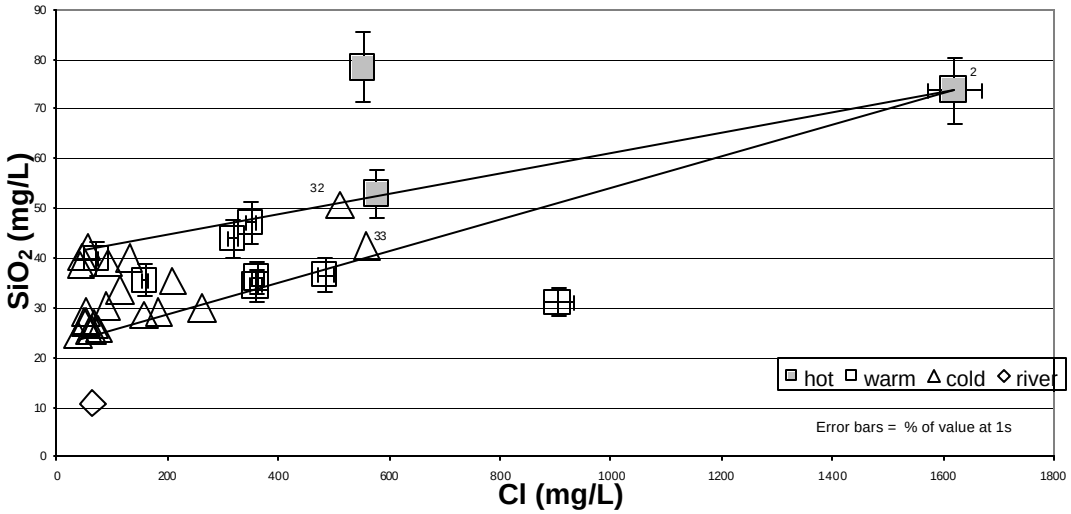

Figure 22 Silica concentration vs. chloride concentration shows a linear mixing trend.

with bromide remaining in the brine. Dissolution and re-precipitation results in even higher Cl/Br ratios (Davis et al., 1997; Hounslow, 1995; and Hanor, 1988). The generally high Cl/Br ratios found in cold-water wells in the Mesilla Basin (349 – 661) could be the result of dissolution of evaporite minerals contained in the basin deposits (Fig. 19). The even higher Cl/Br ratio (1350) in MV2 (the geothermal end member) can be attributed to geochemical processes along deep regional flow paths, in which water typically progresses from bicarbonate through sulfate to chloride in anion character with increasing depth (Toth, 1999; Mazor, 1997). The result is that the difference in Cl/Br ratio can be used to distinguish local aquifer waters from geothermal waters and to indicate mixtures of the two.

Figure 19 shows that the waters of the Mesilla Basin fall into two distinct mass ratio groups. This indicates that the cold and warm waters in the group with higher Cl/Br ratio are a mixture containing a component of geothermal water. The Cl/Br (Fig. 19) ratio shows that Wells MV1, 3, 5, 6, 17, 18, 19, 31, 34 and 36 could be mixtures of the geothermal water with Mesilla Basin waters. Figure 23 shows bromide concentration as a function of chloride concentration, which supports this interpretation, although the scale has been changed so that MV1 and 2 are out of view. Also shown are evaporation lines for the river and dilute cold waters. The evaporation lines were

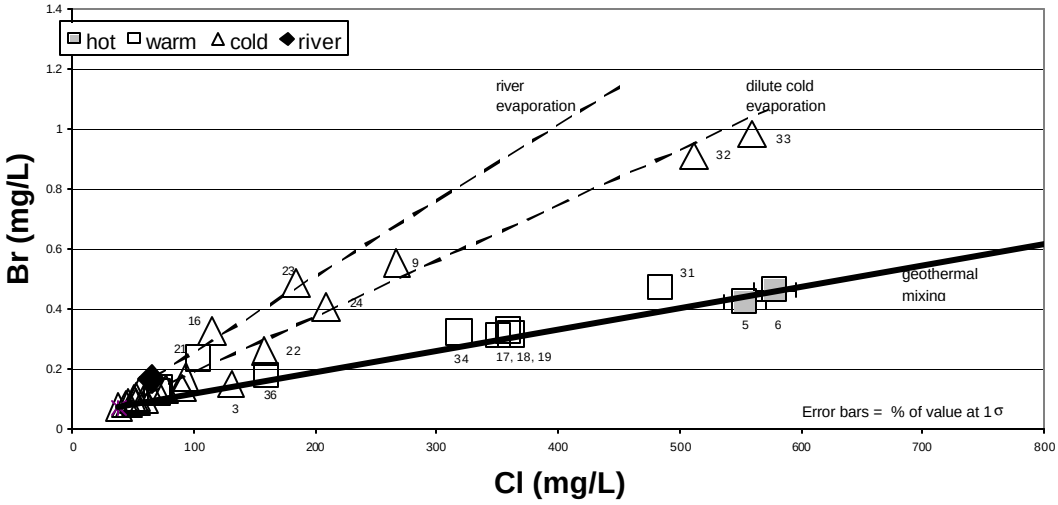

Figure 23 Bromide concentration vs. chloride concentration shows multiple linear mixing or evaporation trends.

constructed using the initial point of river and dilute water and the principal that reducing the solute by half will result in a doubling of the ion concentrations (Anderholm, 2002). The evaporation lines may explain higher bromide concentrations in wells MV9, 16, 21, 22, 23, 24, 32 and 33. An alternative cause for the high bromide concentrations of these wells could be mixing with another geothermal end member that was not sampled.

Chloride/Sulfate Ratio

The chloride/sulfate (Cl/SO_4) ratio, calculated from milli-equivalents per liter, is commonly high in geothermal wells. Gross (1988) compared the Cl/SO_4 ratio for geothermal wells near MV5 and 6 with values found in cold-water wells of the Mesilla Valley. He plotted all the wells on an area map, distinguishing those with ratios greater than one standard deviation above the Mesilla Valley cold well average. His conclusion was that the higher ratios were in geothermal wells and cold wells near the boundary of the geothermal field. Using the same method as Gross but a larger data base consisting of values for 514 Mesilla Valley cold wells (USGS, 2000), an average Cl/SO_4 ratio of 2.02 with standard deviation (σ) = 2.0 was calculated. All of the hot and most of the warm wells in this study had values greater than 4.02 (the Mesilla Valley average plus one standard deviation). Additionally, cold wells MV 3, 32, and 33 had ratios greater than 4.02,

indicating that all of these are included in the mixed water group. Three of the warm wells, MV 21, 29 and 35 have ratios below 4.02, and thus do not appear to be mixtures. Caution must be exercised, however, as the fingerprint diagrams indicate that sulfate levels may be modified by dissolution reactions after mixing.

Lithium

As early as 1957 White discussed high levels of lithium in geothermal waters. A short time later Ellis and Wilson (1960) noted a correlation between lowest Na/Li ratio and highest temperature zones in a geothermal field, a result of high Li in geothermal waters. The linear appearance of Figure 20 gives an immediate impression that many wells in this suite are a result of mixing of cold waters with the geothermal end member. Warm wells (except MV21, 29, 35, and 36) and cold wells MV9, 32 and 33 could all represent mixtures of these waters.

Silica

Two mixing lines have been added to Fig. 22 between MV2 and the low and high cold end members. These mixing lines indicate that most of the warm wells could be mixtures of the hot and cold waters of the basin.

Mahon (1966) first recognized a relationship between silica and temperature in geothermal fluids. Since then Fournier and his

coworkers have developed this relationship into several equations that can be used for geothermometry in different geologic situations; none, however, remains accurate when the geothermal sample is mixed after leaving the geothermal reservoir and cooling (Fournier and Rowe, 1966; Fournier and Marshall, 1983; Fournier and Potter, 1982a,b). Silica is more soluble in water at high temperature and reacts slowly at low temperature so that geothermal waters retain high silica concentrations even after cooling. This statement is an oversimplification for geothermometry, but will do for the purposes of determining water mixing. Because the silica levels alone do not distinguish well between the hot and cold waters of this suite, the Cl/SiO_2 ratio (from mg/L) is plotted as a function of the chloride concentration (Fig. 24). This shows a linear trend with the hot wells and most of the warm wells plus cold wells MV9, 32 and 33 above the Cl/SiO_2 ratio of 7.0 while all other wells are below 7.0. Again warm wells MV21, 29, 35 and 36 fall into the lower ratio group along with most of the cold-water wells.

Summary

In summary, the trace elements tend to support the division of wells into related water types as noted in the Piper analysis of the major elements. Piper calcium type water includes the cold-water wells plus warm-water well MV21, while alkali type water includes the

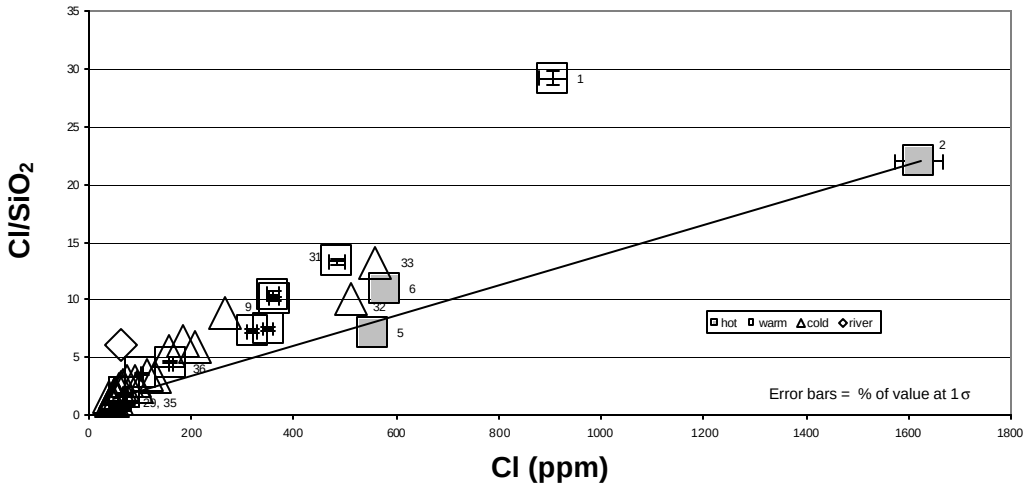

Figure 24 Chloride/silica ratio vs. chloride concentration shows a linear mixing trend.

hot and warm-water wells plus cold wells MV32 and 33. The trace elements generally support this division with few exceptions. The Cl/SO_4 ratio and the Cl/Br ratio would add cold-water well MV3 to the list of mixed waters. Lithium, Na/Li ratio would add cold well MV9 to the mixed type waters. Alternatively, warm-water wells MV29, 35 and 36 do not appear to be related to the mixed waters, MV29 supported by all of the trace element methods and MV35 and 36 supported by all except the Cl/Br ratio. In addition to the methods already discussed isotope data can be used to determine mixing of waters.

Isotopes

Hydrogen and Oxygen

The stable isotopes of hydrogen (^1H) and deuterium (^2H or D), and oxygen (^{16}O and ^{18}O) occur in nature at fixed ratios. For both hydrogen and oxygen, the light isotope makes up more than 99% of the total with the heavier isotope constituting less than 1%. Because the mass of atoms is made up almost entirely of the protons and neutrons contained within the nucleus, the addition of a neutron to a hydrogen atom to form deuterium nearly doubles the mass. In oxygen the addition of two neutrons to form ^{18}O increases the mass by approximately 12.5%. These mass differences are sufficiently significant to cause the isotopes to undergo physical reactions at

different rates and thus to result in measurable fractionation. This is particularly true in water, which is made up of only hydrogen and oxygen atoms. The hydrologic cycle fractionates the light from heavy water molecules during the processes of evaporation and condensation; lighter molecules evaporate more easily and heavy molecules condense more favorably (Mazor, 1997; Gat, 1996; Faure, 1986).

By convention, delta (δ) notation is used with isotopes. Delta is the comparison of the ratio of heavy to light isotopes in the sample compared to a standard. For both hydrogen and oxygen, standard mean ocean water prepared for the International Atomic Energy Agency in Vienna (VSMOW) is used as the standard. The delta of the heavy isotope of hydrogen and oxygen are given as per mil (‰) differences to VSMOW:

$$\delta D\ ‰ = \frac{(D/H)_{sample} - (D/H)_{VSMOW}}{(D/H)_{VSMOW}} * 1000$$

$$\delta^{18}O\ ‰ = \frac{\left(^{18}O/^{16}O\right)_{sample} - \left(^{18}O/^{16}O\right)_{VSMOW}}{\left(^{18}O/^{16}O\right)_{VSMOW}} * 1000$$

Enrichment of the heavier isotope with respect to the standard is indicated by positive values of δD and $\delta^{18}O$, and depletion by negative values (Mazor, 1997; Gat, 1996; Faure, 1986).

Valuable information can be gained from δD vs. $\delta^{18}O$ graphs like Figure 25. Craig (1961) published a global meteoric water line (GMWL) based on a large number of analyses from around the world. Although there are isotopic variations in local rainfall caused by temperature, severity of rainfall, relative humidity, and other factors, the GMWL is an average for precipitation around the world and falls along the line $\delta D = 8 * \delta^{18}O + 10$. Other authors have published meteoric water lines (MWL) for both large and local areas, which commonly fall along lines with slopes near 8 but with δD intercepts that are quite variable (Mazor, 1997; Gat, 1996; Faure, 1986). Dansgaard (1964) found that temperature was the major determining factor for the magnitude of isotope depletion for precipitation with several other factors producing smaller changes. These factors include the effect of: 1) altitude--higher altitudes receive isotopically lighter precipitation; 2) amount--precipitation becomes isotopically lighter through time in a given storm; 3) continental effect--greater distances from coast receive isotopically lighter rainfall; 4) seasonal variations--winter rains are isotopically lighter than summer; and 5) paleoclimate--rainfall of cooler climatic conditions are isotopically lighter than those of warmer periods (Fontes, 1980).

Two natural reactions cause isotope values to fall to the lower right of the meteoric water line (MWL). First, evaporation lines can be

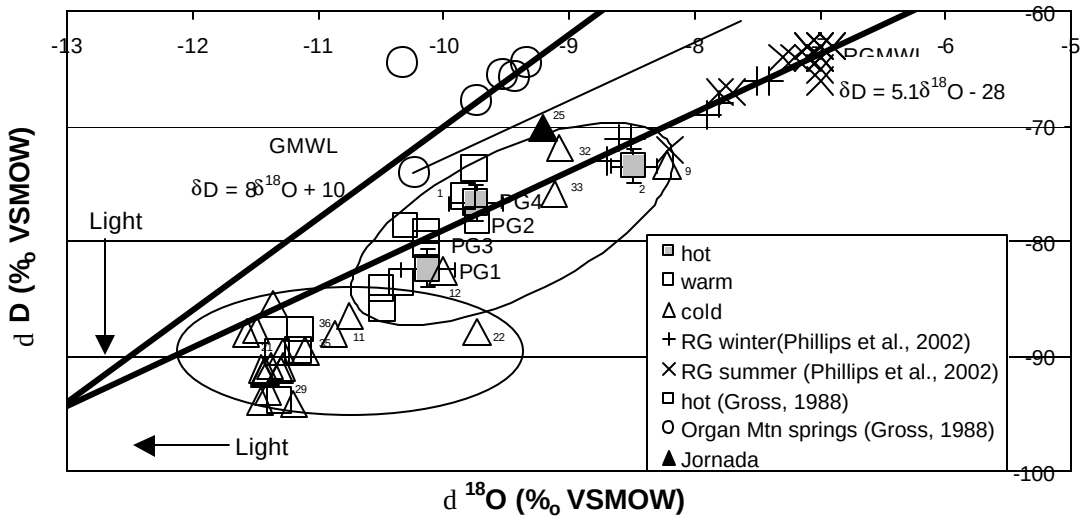

Figure 25 δD vs. $\delta^{18}O$

detected in residual waters that attain heavier characters as a result of preferential evaporation of lighter molecules from the surface of water bodies. Normally these residual waters plot along an 'evaporation line' with a slope in the range of two to five. Second, geothermal waters above 60 – 80 ^{o}C will exchange ^{18}O with rocks during long periods of water-rock interaction; this exchange will produce waters with heavier δ^{18}O values. These waters typically plot horizontally to the right of the meteoric source water, because there is very little hydrogen in rocks to change δD values. The amount of oxygen exchange determines the distance moved from the original water, and is a function of rock composition, texture, temperature and length of contact (Mazor, 1997; Gat, 1996; Nicholson, 1993: Fontes, 1980).

Results

No specific water line has been published for the Mesilla Valley. Vuataz and Goff (1986) determined a local meteoric water line for the Jemez Mountains region in central New Mexico to be parallel to the GMWL with a deuterium excess of +12 (i.e. $\delta D = 8\ \delta^{18}O + 12$). The Vuataz and Goff line was established using 36 samples from 28 locations in the Jemez Mountains. Gross (1988) provides isotope measurements for six springs in the Organ Mountains on the eastern edge of the Mesilla Basin. When plotted with the data obtained in this

study (Fig. 25), the Gross data appears to be offset further to the right of the GMWL. His data also contain values for NMSU geothermal production wells, PG2 and PG3, while this study contains values for PG1 (MV5) and PG4 (MV6). All four of these wells are in close proximity, and because they all contain a component of geothermal water, which presumably comes from the same source, they should all have similar $\delta^{18}O$ values, but the Gross values are much heavier. The difference is possibly related to different methods used to analyze the samples or to the standards used. Subtracting a constant of 3.73‰ from the $\delta^{18}O$ values of Gross aligns these four geothermal samples. Applying the same constant to the six Organ Mountain spring sample values suggests that the Organ Mountain meteoric water line falls on the GMWL of Craig (1961) (Fig. 25). Also plotted in Figure 25 is the Rio Grande Mean Water Line of Phillips et al. (2002) at $\delta D = 5.1\ \delta^{18}O - 28$. It represents an evaporation line based on river samples taken at regular intervals along approximately 1,200 km of the Rio Grande from Colorado to Texas. Several points from Phillips et al. (2002) for Rio Grande sample locations within the Mesilla Basin are plotted in Figure 25. These points are all heavier (more positive) in both δD and $\delta^{18}O$ than any well samples taken from within the basin. The heaviest samples from this suite, wells MV2, 9 and 32 (Table 4), plot with the lightest Rio Grande waters within the basin.

The geothermal hot and most warm wells are isotopically heavier than the cold wells. The exceptions are warm wells MV21, 29, 35 and 36, which plot with the cold wells, and cold wells MV9, 12, 32 and 33, which are isotopically heavier. Well MV22 has a high $\delta^{18}O$ for its δD causing it to lie to the right of most of the cold well group. The data of Gross (1988) had a similar single variation, which he explained as natural variation in the cold wells of the basin.

Discussion

The relative position of samples on the δD-$\delta^{18}O$ graph (Fig. 25) can provide information on the origin of water. If the Organ Mountain springs sampled by Gross (1988) represent regional meteoric water, then these samples represent the heaviest source water in the area. Because of the arid climate of the region, most water is subject to evapotranspirative processes resulting in progressively heavier residual water through time with greater evaporation, as proposed by Phillips et al. (2002) for the Rio Grande trend. A parallel line to the Rio Grande evapotranspiration trend has been added to Fig. 25 from the lightest of the Organ Mountain spring waters, this trend line passes very close to sample MV25, a well located on the Jornada del Muerto, showing recharge of this well from a recent meteoric source. The very low δD and $\delta^{18}O$ values of the Mesilla Basin cold wells indicates that these wells were not recently recharged directly from

either meteoric water or river water, both of which are heavier. Because the wells are lighter than both modern sources, the Mesilla Basin well waters probably represent paleowaters from precipitation during a much cooler climatic period (Plummer et al., 2000 and Scanlon et al., 2001).

Because $\delta^{18}O$ does not chemically fractionate to great extent at temperatures below 80 ^{o}C, the warm waters could be interpreted to represent mixtures between geothermal and cold end members (Fig. 25). However, because the geothermal end member and the river samples plot in the same direction from the cold wells, mixtures could also represent cold wells mixing with either river water or geothermal water. Musgrove and Banner (1998) demonstrated that δD and $\delta^{18}O$ can be plotted against another conservative ion such as chloride, which results in the end members being more easily distinguished (Fig. 26 and 27). Figures 26 and 27 show MV2 as the geothermal end member for the warm wells. Connecting the three end members (MV2, MV10, and the river) with straight lines shows that the isotopic composition of most of the wells in the basin can be explained by mixtures of the three end members. More specifically, in Figure 27 cold wells MV9, 11, 12, 22, 32 and 33, and warm well MV17 show an influence by water from the Rio Grande. Figure 26 confirms that waters from the Rio Grande influence cold wells MV9, 11, 12, 32 and

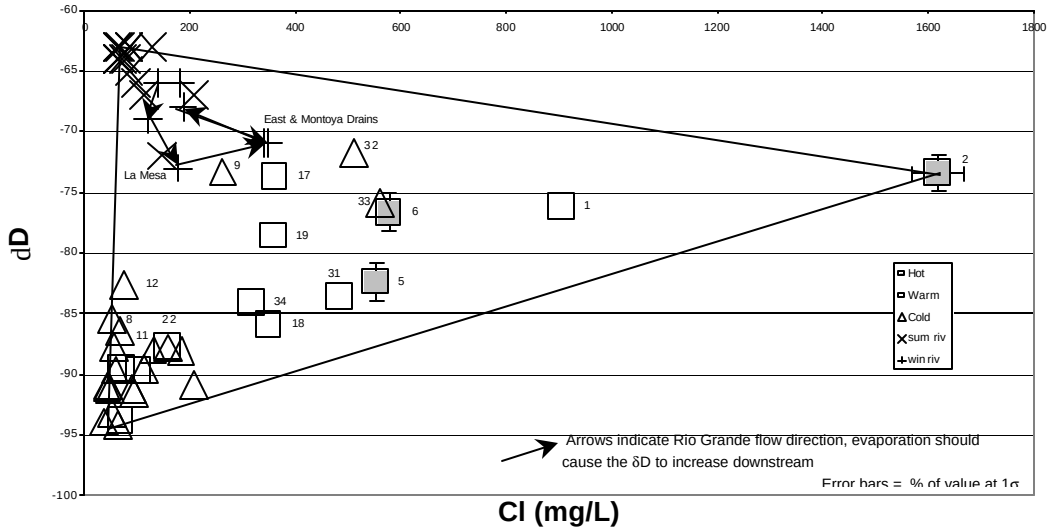

Figure 26 δD vs. chloride concentration

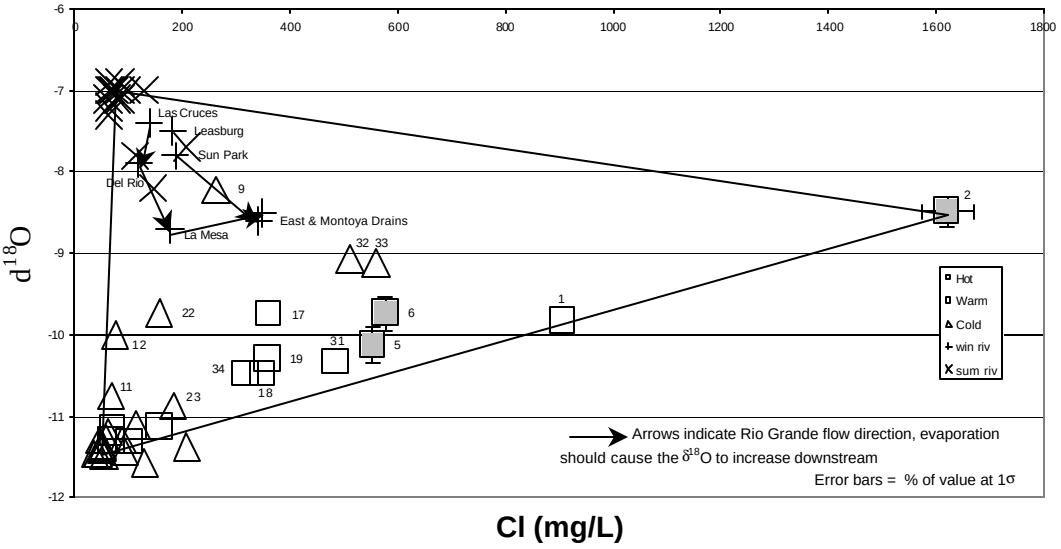

Figure 27 $\delta^{18}O$ vs. chloride concentration.

33, and warm well 17. Figure 26 also shows a possible influence on wells MV6, 8 and19, but does not show an influence on well MV22. Figures 26 and 27 suggest that wells MV9, 17, 32, 33 and possibly 6 and 19 are mixtures of all three end-members. Because of their locations, wells MV6, 17, 19 and 22 appear unlikely to be influenced by direct river input. Closer inspection of the Rio Grande data points of Phillips et al. (2002) suggests that mixing with ground water is also influencing the composition of the river water.

Evaporation causes the residual Rio Grande water to become isotopically heavier as it flows southward from its headwaters in Colorado to its terminus in Texas. This isotopic increase is described by the RGMWL of Phillips et al. (2002) shown in Figure 25. However, in figures 26 and 27 the Mesilla Basin segment of the river shows several reversals with lighter water downstream. The geographic sequence of sample locations and approximate distances between is shown in Table 5 and Figure 28.

Sample location	Distance downstream from preceding sample (km)
Leasburg Dam	
Las Cruces	15
Del Rio Drain	15
La Mesa Drain	10
East Drain	10
Sunland Park	20
Montoya Drain	5

Table 5 Phillips et al. (2002) Rio Grande sample locations in the Mesilla Basin

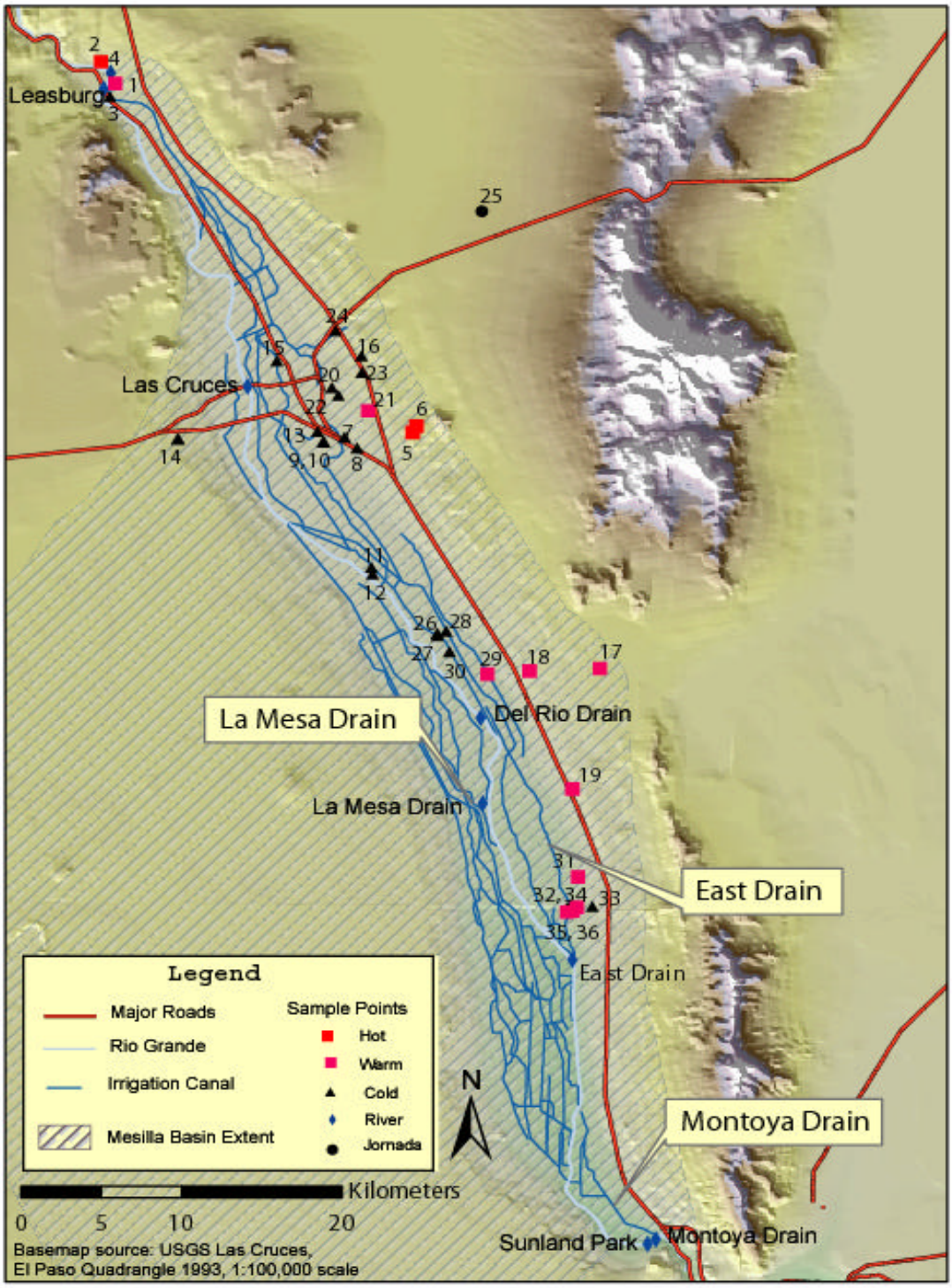

Figure 25 Map showing Rio Grande sample locations of Phillips et al. (2002) and irrigation canals in the Mesilla basin.

Figure 29 shows the δD vs. $\delta^{18}O$ for the Mesilla Basin section of the Rio Grande for winter samples only with arrows showing the flow vector from Leasburg Dam to Montoya Drain. River isotopes are the heaviest in samples collected at Leasburg, where water enters the basin and at Las Cruces, the next station downstream. Several samples taken south of Las Cruces show a reversal in the evaporative trend with the La Mesa sample becoming the lightest. Sunland Park samples, however, are heavier than samples to the north and south; representing another trend reversal. The lighter samples south of Las Cruces must represent the inflow of isotopically lighter ground water to the river. The inflow of isotopically lighter ground water is enough to reverse the evaporative trend even during the heavy summer flow, and because there is a corresponding increase in the chloride concentration the input appears to be contributed via the La Mesa and Montoya drains. An examination of the canals in Figure 28 shows that the La Mesa and Montoya drains flow through areas of where geothermal groundwater is mixing with isotopically lighter basin water and could be entering the drains to input both increased chloride and lighter isotopes to the river. The trend reversals can be followed in Figs. 26 and 27, from La Mesa Drain to East Drain the samples become isotpically heavier and higher in chloride, this could represent the addition of a mixture containing a greater proportion of

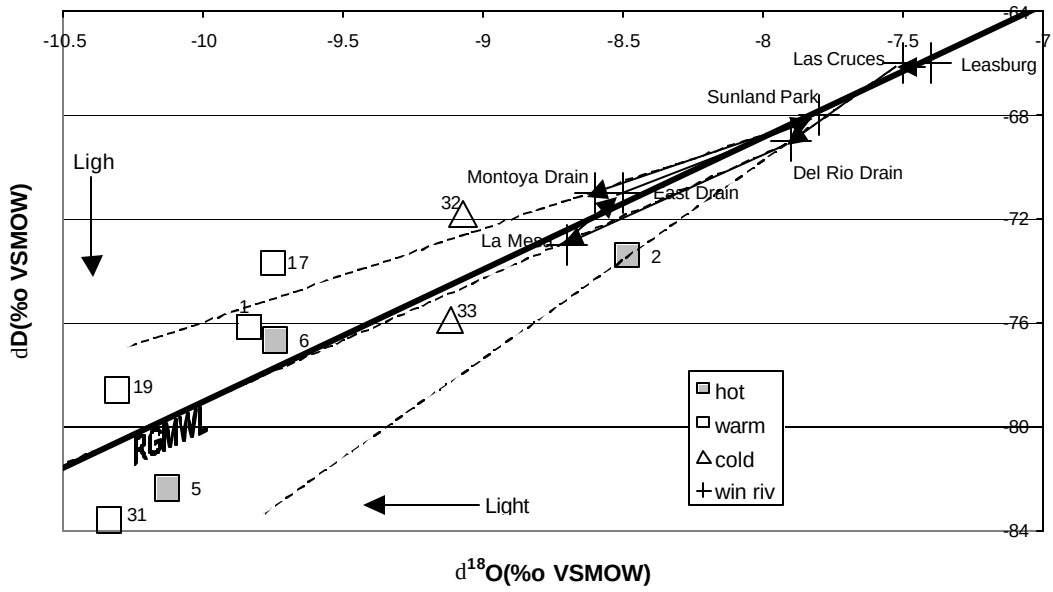

Figure 29 δD vs. $\delta^{18}O$ for Rio Grande samples

geothermal with less basin water. At Sunland Park the river is isotopically heavier with less chloride indicating an input from irrigation drains without a geothermal mixture addition. However, the isotope chloride trends reverse again within the 5 km from Sunland Park to Montoya Drain, indicating another geothermal/basin mixed ground water addition. Extensions of the trend lines, shown in Figure 29, between points indicating possible mixing with isotopically lighter water indicate that basin water similar to those sampled could provide the lighter isotopes. Figures 26 and 27 show that a mixture of geothermal with cold ground water is the likely source of the lighter isotopes and increased chloride between Las Cruces and Montoya Drain sample points.

The close correlation that is shown between chloride concentration and electrical conductivity in figure 6, results in the same pattern of reversals when δD is plotted as a function of EC (Figure 30). This is a valuable relationship because it will allow researchers to use an inexpensive field meter to more accurately locate areas where geothermal water is entering the irrigation drainage system and the Rio Grande.

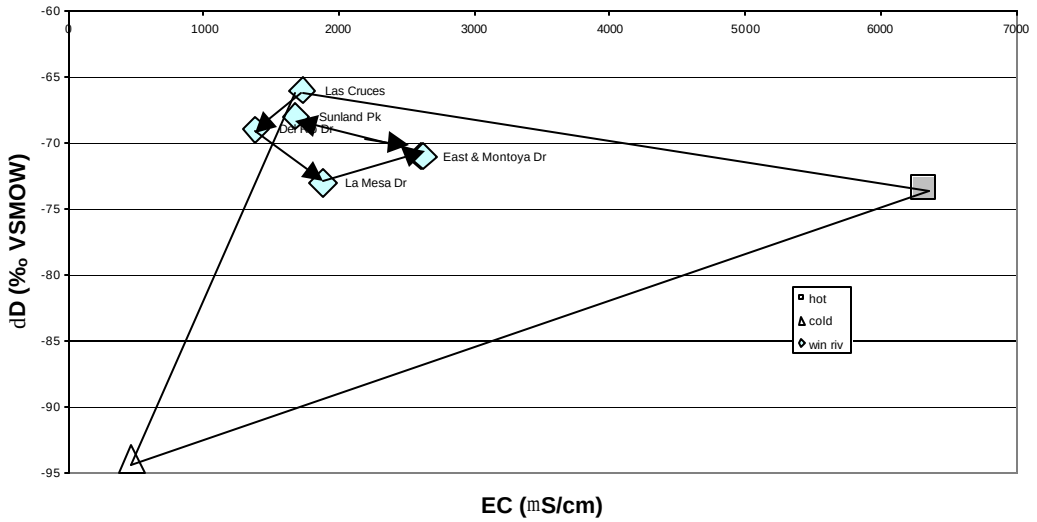

Figure 30 δD vs. EC, shows the pattern of downstream δD reversals

Carbon ($\delta^{13}C$)

Carbon, like hydrogen and oxygen, has multiple isotopes. In the case of carbon the isotopes of ^{12}C and ^{13}C are stable while the ^{14}C isotope is radioactive. In this study only the stable isotopes were measured, and are reported using the same delta notation that was used for hydrogen and oxygen isotopes, using the PDB (Peedee Formation belemnites) standard (Faure, 1986). Carbon-12 is the most abundant at 98.89 %, with ^{13}C making up 1.11% of the total isotopes. Carbon isotopes are fractionated by a variety of natural processes, including plant photosynthesis and isotope exchange reactions between carbonate minerals.

Plant photosynthesis can be important in geological processes as a result of organic carbon inclusion in petroleum and coal, both of

which are enriched in ^{12}C (Faure, 1986). Organic carbon can also be incorporated into ocean and lake sediments that undergo diagenesis to form sedimentary rocks. Hoefs (1997) describes two separate pathways for diagenesis, a meteoric pathway for shallow diagenesis that includes meteoric waters and a burial pathway for deep-sea environments. The burial pathway results in carbonates enriched in ^{13}C from fractionation by methane production at burial depth; even when original sediment is light $\delta^{13}C$ organic carbon. The resulting carbonates have high $\delta^{13}C$ values, which average 0.56 ± 1.55 ‰ (Faure, 1986 and Hoefs, 1997).

Results

The results of the $\delta^{13}C$ analyses are shown in table 4 and Figure 29. The geothermal wells have the highest values (– 1.3 to +2.2‰) with intermediate values in warm wells MV1, 17 and 18, and cold well MV33 (– 3.1 to –1.8‰). All other wells fall into a large cluster with values less than –4‰.

Discussion

Geothermal water picks up a distinct carbon signature as a result of water-rock interaction. The geothermal water of well MV2 is enriched in ^{13}C at +2.2‰. This may indicate that the water

underwent water-rock equilibration, in its deep regional flow path, with marine carbonates, which have high $\delta^{13}C$ values and are present in the Cambrian to Permian sedimentary strata of this region. The cold ground waters of the Mesilla Basin have a characteristically more negative $\delta^{13}C$, or greater enrichment in carbon-12. In Figure 31 the $\delta^{13}C$ value is plotted against the chloride concentration. The graph indicates that most of the warm wells and some cold wells may result from mixing between cold and geothermal waters.

Strontium ($^{87}Sr/^{86}Sr$) Ratio

Strontium is a divalent ion that frequently replaces calcium in mineral structures due to its similar ionic radius. Strontium has four stable isotopes: ^{84}Sr, ^{86}Sr, ^{87}Sr, and ^{88}Sr. The natural concentration of ^{87}Sr isotope slowly increases, as it is a product of the beta decay of ^{87}Rb (rubidium), which has a half-life of approximately 48.8×10^9 years. Due to the method used for measuring isotopic ratios it is convenient to report the results as fractions or ratios of two isotopes. The strontium ratio that is most commonly used is $^{87}Sr/^{86}Sr$ (Faure, 1986; Capo et al., 1998 and Stewart et al., 1998).

The strontium ratio is not affected by fractionation during physical processes like the isotopes of the lighter elements. The strontium ratio is set by the availability of isotopes at the time of mineral formation. Because rubidium is monovalent and has an ionic

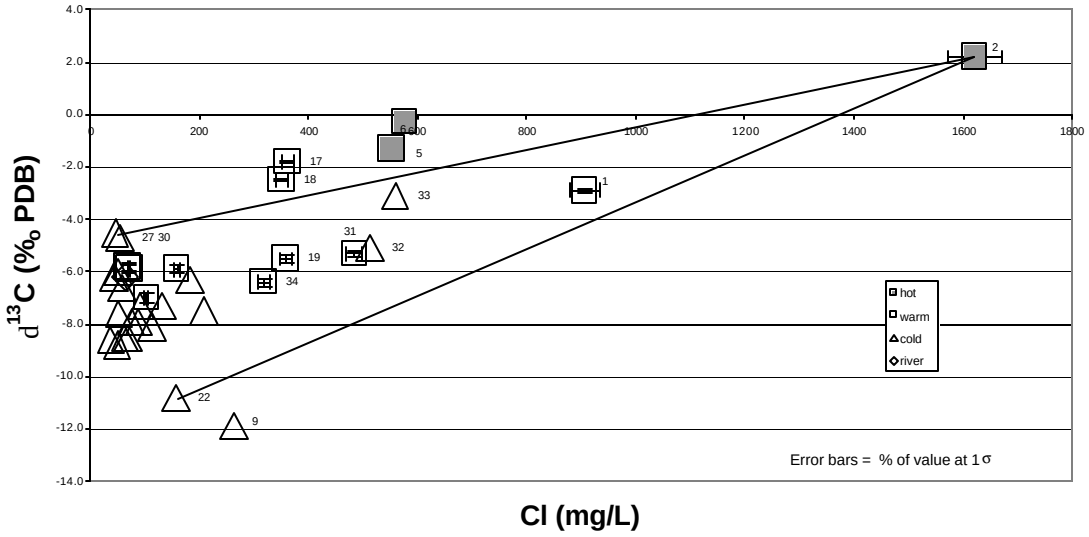

Figure 31 $\delta^{13}C$ vs. chloride concentration shows a linear mixing trend.

radius similar to potassium, it frequently substitutes for potassium in minerals, while strontium substitutes for calcium. As the rubidium decays over time, the quantity of ^{87}Sr and its ratio to other strontium isotopes in the mineral increase. Thus those minerals with high potassium content will generally have high ^{87}Sr contents.

Results

The strontium ratios for this suite are shown in Table 4. When ratios are plotted as a function of the reciprocal strontium concentration mixtures fall on straight mixing lines between end members. Figure 32 shows the geothermal end member well MV2 has the highest ratio at 0.7170, followed by the other geothermal wells at nearly 0.7139. The cold wells plus warm wells MV21, 35 and 36 have values below 0.711. The majority of warm wells have intermediate values between 0.7113 and 0.7134; included in this group are cold wells MV3, 30, 32 and 33.

Discussion

Minerals have characteristic ratios or ranges of ratios dependent upon source, composition and age (Stewart et al., 1998). Burke et al. (1982), for instance analyzed the change in $^{87}Sr/^{86}Sr$ for Paleozoic marine samples, which reflects the seawater strontium and rubidium content at the time of formation. During the Pennsylvanian, average $^{87}Sr/^{86}Sr$ in marine samples was between 0.7080 and 0.7085,

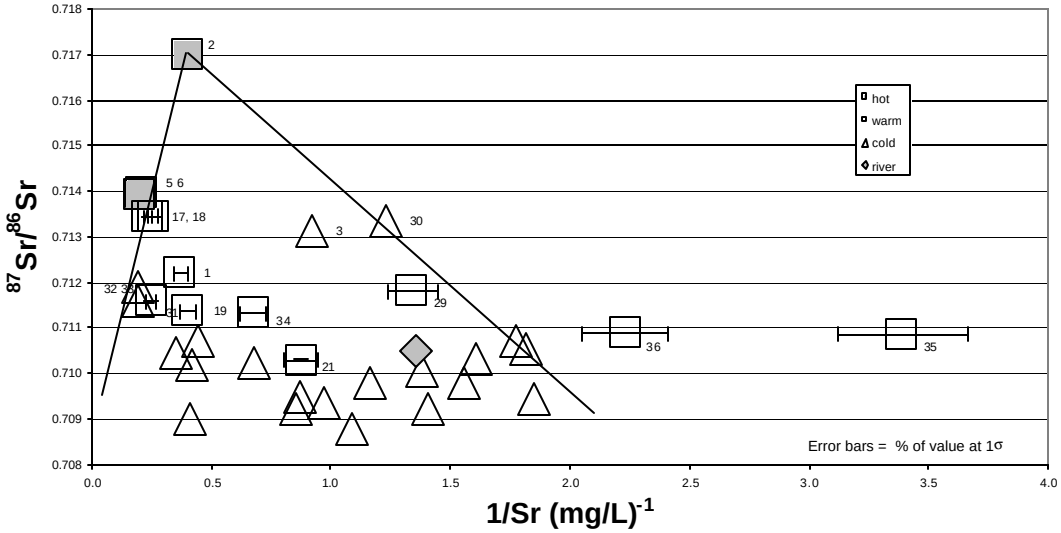

Figure 32 $^{87}Sr/^{86}Sr$ vs. reciprocal strontium concentration shows a range of possible mixing trends.

with one sample being slightly above 0.7090. The fact that the geothermal end member water in this suite has a value of 0.717 contradicts the $\delta^{13}C$ evidence for Pennsylvanian marine carbonates being the source formation of this water. However, Precambrian basement granite in this area has a strontium ratio today of 0.81116 (Butcher, 1990). It is likely that the flow path of the geothermal water allowed the $^{87}Sr/^{86}Sr$ to equilibrate with older, deeper Precambrian basement, 0.81116, and then pass into younger, shallower marine carbonate where the $\delta^{13}C$ re-equilibrated. Because the marine carbonate has a lower $^{87}Sr/^{86}Sr$ (0.708) than the Precambrian granite equilibrated water (0.81116) it would modify the ratio downwards but never reaches a value as low as the marine carbonate. Because there is no mechanism to remove the high ratio strontium already present, the value can only be diluted, thus an intermediate strontium ratio (0.717) results. Alternatively the $^{87}Sr/^{86}Sr$ ratio could be in equilibrium with the basin lithology of the aquifer. The aquifer lithologies consist of aggregate clasts from sources including marine carbonates and Precambrian granites as well as many other sources. This conglomerate could have a $^{87}Sr/^{86}Sr$ ratio at any level between 0.708 and 0.81116, which are most likely the extreme low and high values.

When the $^{87}Sr/^{86}Sr$ is plotted against the reciprocal of strontium concentration, the product of mixing two end members will fall on a straight line connecting those end members. Figure 32 shows that most of the warm wells in this study could be the result of mixing between the geothermal end member and one of the heterogeneous cold waters in the basin. Figure 33 shows δD as a function of the $^{87}Sr/^{86}Sr$ ratio. Mixing lines are shown to indicate mixing taking place between MV2 and cold waters to produce warm waters, and also river input that is influencing cold wells MV9, 11, 12, and 22, and cold wells MV32 and 33.

Summary

The isotope data support the division of wells previously shown by major and trace element data, and provide new information on water source and mixing. The low δD and $\delta^{18}O$ values show that the cold groundwater comes from paleo recharge during a cooler climate rather than current meteoric or river recharge. The geothermal water comes from deep regional flows that account for high chlorine content. The thermal waters chemically interact with Precambrian granite acquiring a high $^{87}Sr/^{86}Sr$ ratio value. The $^{87}Sr/^{86}Sr$ value is modified downwards when the thermal water re-equilibrates with shallower marine carbonate. More importantly, the isotope data show

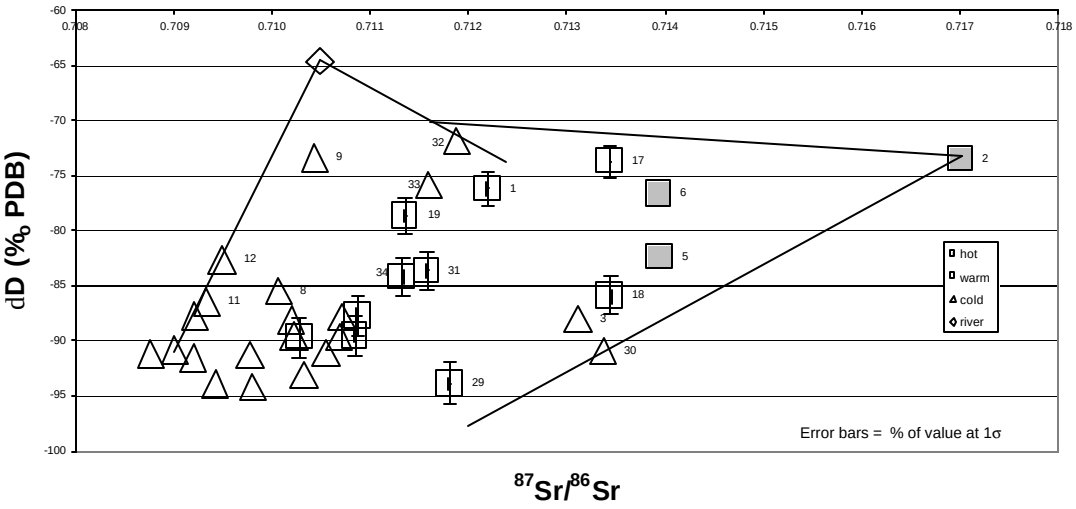

Figure 33 δD vs. $^{87}Sr/^{86}Sr$ shows the influence of both river and geothermal mixing with Mesilla Basin waters.

that several wells and river samples are the result of mixing between all three end members: cold aquifer water, river and geothermal.

Mixtures

Mixtures of geothermal and cold water will result in warm waters with ion concentrations equal to the sum of the product of the ion concentration and proportion of each end member, for example:

$$[Cl]_{warm} = X*[Cl]_{hot} + Y*[Cl]_{cold}$$

Where X and Y represent the proportion of Cl in the hot and cold end members respectively. Fingerprint diagrams, however, have shown that some ion concentrations can be modified after mixing has occurred by reactions with the local lithology. Warm mixed waters can also lose heat while maintaining mixed ion concentrations, like wells MV32 and 33. Other waters have higher temperatures from conductive heating by subadjacent confined thermal aquifers without acquiring the chemistry of mixed water such as wells MV21, 29, 35 and 36. These wells are all located in relatively close proximity to other hot or warm wells in this suite.

The proportion of geothermal water in a warm-water mixture can be calculated with compositional diagrams. Figure 34 shows the most ionically extreme hot (MV2) and cold (MV10) wells used as end points. The two end-members and all warm wells are re-plotted with a mixing line connecting the end members. Distances are calculated

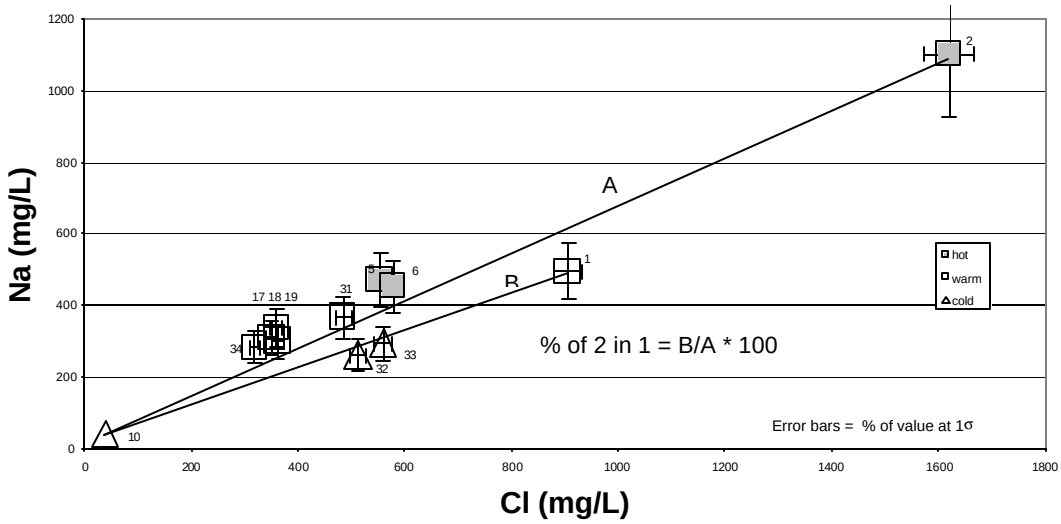

Figure 34 Two end-member mixing

from the cold end member to each warm well and to the hot end member. The percentage of hot water in each warm water is calculated by the equation: $\% = 100 * \frac{d_{warm}}{d_{hot}}$. Where d_{warm} and d_{hot} are distances from the cold end-member to a warm well and the hot end-member respectively (Fig. 34). Several iterations were calculated using Br, Li and Na as a function of both Cl and TDS. Table 6 shows the result as the average percentage of MV2 in each warm well. Several factors should be remembered when viewing these results. First, MV2 could be a mixture of cold basin water with more extreme geothermal water, the true end point for all basin mixed waters, requiring an even smaller percentage of the more extreme geothermal water to create these mixtures. Second, by using the most extreme cold water in the basin the percentages of MV2 shown are maximums; if MV2 mixes with any water with higher concentrations the cold end point moves closer to MV2 and the percentage of MV2 is less. Third, the values found when using TDS are consistently larger than those found when using Cl; this is most likely a result of an increase in TDS from sources other than the mixing of end members. Fourth, those mixtures with less than 10% of MV2 (MV21, 29, 35 and 36) are within the natural variation of cold basin waters. Three end-member mixing can further clarify some of the variations seen in this method.

Well	TDS Average (%) of MV2	TDS σ (%)	Chloride Avg (%) of MV2	Chloride σ (%)
MV1	56	1.9	54	2.0
MV5	46	6.7	34	1.5
MV6	44	5.3	35	0.9
MV17	33	6.4	21	0.8
MV18	32	6.1	20	1.1
MV19	27	3.5	21	1.5
MV21	5	0.7	4	0.3
MV29	7	2.3	3.3	2.2
MV31	37	4.4	29	0.5
MV32	35	3.2	29	1.4
MV33	36	2.5	32	1.4
MV34	22	1.9	18	1.0
MV35	5	1.4	3	1.7
MV36	10	1.0	8	0.8
averages of Br, Li, and Na as a function of TDS and Cl.				

Table 6 Average percentage of MV2 in mixed water compositions

The three end members found in Figures 26 and 27 can be used to calculate the proportion of Rio Grande water in cold-water samples as well as geothermal water in Rio Grande samples along its course through the Mesilla Valley. In Figure 35 the end members have been plotted in terms of the most conservative ions, Cl against δD, and connected to form a mixing triangle. The cold-water and geothermal water end-members are MV10 and MV2, respectively, as were used in the two end member calculations above. The Rio Grande end member is the Las Cruces winter sample of Phillips et al. (2002). The Las Cruces value is used because the trend reversals that were discussed above occur downstream of this sampling point. The end members are connected to form a triangle, and mixing lines have been drawn from the end members through the sample values to the opposite side

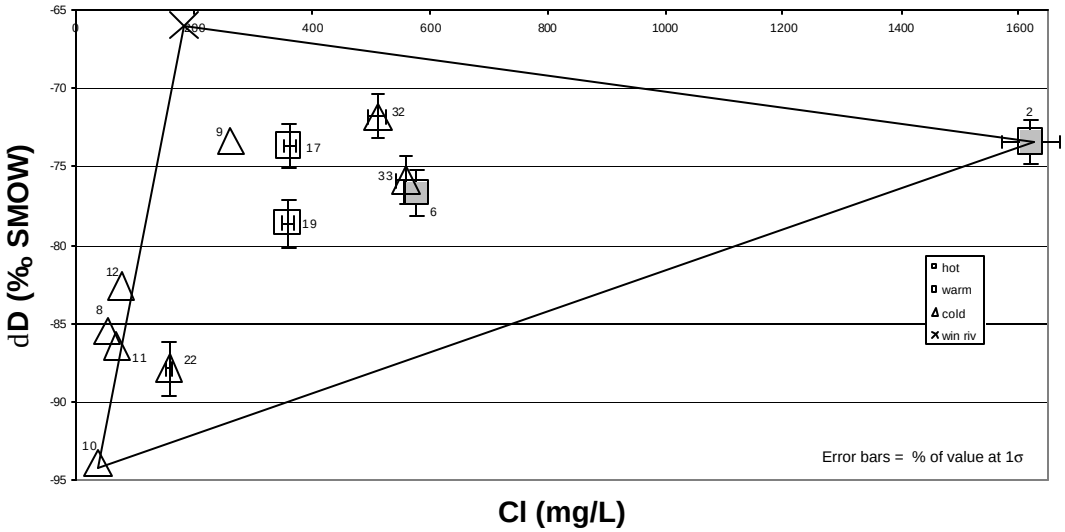

Figure 35 Three end-member mixing diagram of Mesilla Basin waters.

of the triangle. The samples considered are those, which appear to have a component of Rio Grande water. By carefully measuring the distances and calculating the proportions the percentage of cold, geothermal and Rio Grande water of each mixture can be determined (Ragland, 1989). Cold well samples MV8, 11, 12 and 22 contain between 25% and 40% Rio Grande water. Table 7 shows the proportions of waters in hot and warm wells.

Well	% hot	% cold	% Rio Grande
MV6	31	29	40
MV9	8	26	68
MV17	15	22	62
MV19	17	40	43
MV32	24	15	61
MV33	29	28	43

Table 7 Percentage of end members contained in warm well waters using a three end-member-model.

These percentages of hot and Rio Grande are maximums because, as in the two end-member determination, using the extreme cold water as the end member results in the mixture indicating minimum cold-water contribution and maximum of the other components. The geographic separation of wells MV6, 17 and 19 from the river, and the absence of drainage canals in these areas make these three end-member mixes highly unlikely, thus there must be some other source for these ions. The same end members can be used to determine the geothermal contribution to the Rio Grande (Fig. 36). East and Montoya Drain sample points, which are the saltiest in winter,

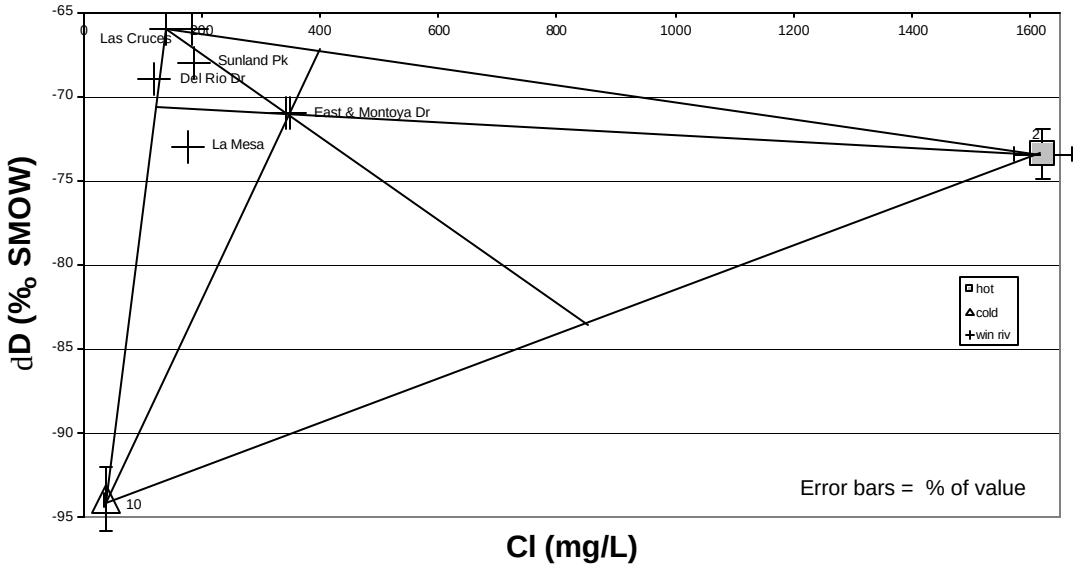

Figure 36 Three end-member mixing diagram of Rio Grande water.

contain approximately 13% geothermal water, 14% cold water and 73% river water. Using the Phillips et al. (2000) summer data shows 9% geothermal in the Montoya Drain sample, but virtually none in the East Drain. The La Mesa Drain sample shows little geothermal input, but 24% cold basin water. Using $\delta^{18}O$ results to perform the calculations results in percentages of geothermal water approximately 2.5% higher than the δD data in winter, but nearly the same for summer.

SUMMARY

In this paper, a variety of parameters and methods have been employed to gain an understanding of the saline contribution from geothermal ground water into the Rio Grande through mixing with cold-water aquifers. Hot and warm waters are found on the northern edge of the basin, in the central basin east of Las Cruces and in the town of Anthony and north about 6.5 km. Major ion chemistry shows two major water groups, calcium waters that comprise most of the cold-water wells, and alkali waters consisting mostly of hot and warm waters. Fingerprint diagrams differentiate the two water groups further and show that high bicarbonate and sulfate concentrations are geographically related. The high bicarbonate and sulfate concentrations may be the result evaporite dissolution and may be modifying warm water mixtures. Identification of mixing trends is attempted using cluster analysis, but is found to be unreliable as tested. Results may be improved by using more major groups or by using more variables. Trace elements are used to confirm the identification of mixed aquifer waters, also showing that some mixed chemistry waters are cold, and that some warm waters do not have chemistries of mixed water. Finally, isotopes of oxygen, hydrogen, carbon, and strontium are used to show that the three major waters of the basin, cold ground water, geothermal water, and river water,

could be mixed in different proportions to produce all intermediate waters within this suite. Several wells (MV9, 12, 22, 32, and 33) show a mixture of all three end-member waters while the river shows evidence of geothermal input, probably in the form of mixed aquifer water. Rio Grande salinity requires less than 15% geothermal contribution to reach its most saline condition. However, the two end-member calculations show that some of the salinity (TDS) is contributed from other sources.

REFERENCES

Alther GA, 1979, A simplified statistical sequence applied to routine water quality analysis: a case history, Ground Water, Vol. 17, p. 556-561

Anderholm, S.K., 1990, Water quality and geochemistry of the Mesilla Basin, in Frenzel, P.F., and Kaehler, C.A., Geohydrology and simulation of ground-water flow in the Mesilla Basin, Dona Ana County, New Mexico, and El Paso County, Texas; U. S. Geological Survey Professional Paper 1407C, p. C64-C78

Anderholm, S.K., 2002, Water-quality assessment of the Rio Grande Valley, Colorado, New Mexico, and Texas – Surface-water quality, shallow ground-water quality and factors affecting water quality in the Rincon Valley, south-central New Mexico, 1994-95, U.S. Geological Survey Water-Resources Investigations Report 02-4188, Albuquerque, NM, 59 p.

Burke, W.H., Hetherington, E.A., Koepnick, R.B., Nelson, H.F. & Otto, J.B., 1982, Variation of seawater $^{87}Sr/^{86}Sr$ throughout Phanerozoic time. Geology. Vol. 10, p. 516-519

Butcher, D., 1990, Geochemistry and Nd-Sr systematics of selected lithologic units of the Oligocene Organ cauldron and batholith, south central New Mexico, MS Thesis, New Mexico State University, Las Cruces, New Mexico, 145 p.

Brown, C.E., 1998, Applied multivariate statistics in Geohydrology and related sciences, Springer-Verlag, Berlin Heidelberg, 248 p.

Capo, Rosemary C., Stewart, Brian W., and Chadwick, Oliver A., 1998, Strontium isotopes as tracers of ecosystem processes: theory and methods, Geoderma, Vol. 82, p. 197-225

Craig, H, 1961, Isotopic variations in meteoric waters, Science Vol. 133, p. 1702-1703

Dansgaard, W., 1964, Stable isotopes in precipitation, Tellus, Vol. 16, p. 461-469

Davis, S.N., Whittemore, D.O. & Fabryka-Martin, J. 1997, Uses of chloride/bromide ratios in studies of potable water, Ground Water, Vol. 36, No. 2, p. 338-350

Ellis, A.J. and Wilson, S.H., 1960, The geochemistry of alkali metal ions in the Wairakei hydrothermal system, New Zealand Journal of Science, Vol. 3, p. 593-617

Faure G., 1986, Principles and applications of geochemistry: a comprehensive textbook for geology students. Prentice Hall, Upper Saddle River, New Jersey, 374 p.

Fontes, J.C.H., 1980, Environmental isotopes in groundwater hydrology, In: Fritz, P. and Fontes, J.CH., eds. Handbook of environmental isotope geochemistry, v. 1, The terrestrial environment: New York, Elsevier, p. 75-140

Fournier, R.O. and Marshall, W.L., 1983, Calculation of amorphous silica solubilities at 25°C to 300°C and apparent cation hydration numbers in aqueous salt solutions using the concept of effective density of water. Geochim et Cosmochimica Acta, Vol. 47, p. 587-596

Fournier, R.O. & Potter, R.W., 1982a, An equation correlating the solubility of quartz in water from 25 °C to 900 °C at pressures up to 10,000 bars. Geochim et Cosmochimica Acta, Vol. 46, p. 1969-1974

Fournier, R.O. & Potter, R.W., 1982b, A revised and expanded silica (quartz) geothermometer. Geothermal Research Council Bulletin, November, p. 3-12

Fournier, R.O. & Rowe, J.J., 1966, Estimation of Underground Temperatures from the Silica Content of water from Hot Springs and Wet Steam Wells, American Journal of Science, Vol. 264, Nov. p. 685-697

Freeze R.A., and Cherry, J.A., 1979, Groundwater: Prentice-Hall, Inc., Englewood Cliffs, New Jersey, 604 p.

Frenzel, P.F., and Kaehler, C.A., 1992. Geohydrology and simulation of ground-water flow in the Mesilla Basin, Dona Ana County, New Mexico, and El Paso County, Texas; U. S. Geological Survey Professional Paper 1407-C, 105 p.

Gat, J.R., 1996, Oxygen and hydrogen isotopes in the hydrologic cycle, Annual Review of Earth and Planetary Sciences, Vol. 24, p. 225-262

Gross, J.T, 1988, A Hydrogeological Investigation of the Las Cruces Geothermal Field, MS Thesis, New Mexico State University, Las Cruces, New Mexico, 212 p.

Guler, C., Thyne, G.D., & McCray, J.E., & Turner, A.K., 2002, Evaluation of graphical and multivariate statistical methods for classification of water chemistry data, Hydrogeology Journal, Vol. 10, p. 455-474

Hanor, J.S., 1988, Origin and Migration of subsurface sedimentary brines, Lecture notes for short course no. 21, Society of Economic Paleontologists and Mineralogists, Tulsa, OK, 230 p.

Harris, L.G., 1996, The Developers: Controlling the Rio Grande 1890-1980, Proceedings of the 40th Annual New Mexico Water Conference, NMWRRI, p. 7-12

Hawley, J.W., Kottlowski, F.E., Seager, W.R., King, W.E., Strain, W.S., and Lemone, D.V., 1969, The Santa Fe Group in the south central New Mexico border region: New Mexico Bureau of Mines and Mineral Resources Circular 104, p. 52-67.

Hawley, John W. and Lozinsky, Richard P., 1992, Hydrogeologic Framework of the Mesilla Basin in New Mexico and Western Texas, New Mexico Bureau of Mines and Mineral Resources New Mexico Institute of Mining and Technology, Open-File Report 323, 55 p.

Hem, J.D., 1985, Study and interpretation of the chemical characteristics of natural water (3rd ed), U.S. Geological Survey Water-Supply Paper 2254, 263 p.

Hoefs, J., 1997, Stable Isotope Geochemistry, Springer-Verlag, Berlin Heidelburg, 308 p.

Hounslow, A.W., 1995, Water quality data: Analysis and interpretation, CRC Press Inc., Boca Raton, FL., 397 p.

Leggat, E.R., Lowery, M.E., and Hood, J.W., 1962, Ground-water resources of the lower Mesilla Valley, Texas and New Mexico: Texas Water Commission Bulletin 6203, 191 p.

Mack, G.H, Kottlowski, F.E. and Seager, W.R., 1998, The stratigraphy of south-central New Mexico, New Mexico Geological Society Guidebook, 49th Field Conference, Las Cruces Country II, p. 135-154

Mahon, W.A.J., 1966, Silica in hot water discharged from drillholes at Wairakei, New Zealand, N.J. Journal of Science, Vol. 9, p. 135-144

Mazor, E., 1997, Chemical and isotopic groundwater hydrology: The applied approach, 2nd ed., Marcel Dekker Inc., New York, 413 p.

Musgrove, M.L. and Banner, J.L., 1993, Regional ground-water mixing and the origin of saline fluids: mid-continent, United States, Science, Vol. 259, p. 18771882

Nickerson, E.L., and Myers, R.G., 1993, Geohydrology of the Mesilla Ground Water Basin, Dona Ana County, New Mexico, and El Paso County, Texas, U. S. Geological Survey Water-Resources Investigations Report 92-4156, 89 p.

Nickerson, E. L., 1998, U.S. Geological Survey seepage investigations of the Lower Rio Grande in the Mesilla Valley, In Water Challenges on the Lower Rio Grande, edited by C.T. Ortega Klett, Proceedings of the 43rd Annual New Mexico Water Conference, New Mexico Water Resources Research Institute Report No.310, p. 59-68.

Ochsenkuhn K.M., Kontoyannakos J., Ochsenkuhn-Petropulu M., 1997, A new approach to a hydrochemical study of groundwater flow, Journal of Hydrology, Vol. 194, No.1-4, p. 64-75

Peterson, D.M., Khaleel, R., and Hawley, J.W., 1984, Quasi three-dimensional modeling of groundwater flow in the Mesilla bolson, New Mexico and Texas: New Mexico Water Resources Research Institute Report 178, 185 p.

Phillips, F.M., Hogan, J.F., Mills, S.K., and Hendrickx, J.M.H., 2002, environmental Tracers Applied to Quantifying Causes of Salinity in Arid-Region Rivers: Preliminary Results from the Rio Grande, Southwestern USA, in Water Resources Perspectives: Evaluation,

Management and Policy, edited by A.S. Alsharhan and W. W. Wood, Elsevier, Amsterdam, 2002, 9 p.

Piper, A.M., 1944, A Graphic Procedure in the Geochemical Interpretation of Water-Analyses, Transactions, American Geophysical Union, Vol. 25, p. 914-923

Plummer, L.N., Bexfield, L.M., S.K. Anderholm, Sanford, W.E., and E. Busenberg. 2000, Geologic and hydrologic framework: C. Geochemical characterization of ground water flow paths in parts of the Santa Fe Group aquifer system, Middle Rio Grande Basin, New Mexico. In U.S. Geological Survey Middle Rio Grande Basin Study—Proceedings of the Fourth Annual Workshop, Albuquerque, New Mexico, February 15-16, 2000. Edited by J.C. Cole. U.S. Geological Survey Open File Report 00-488, p. 7-12.

Ragland, P.C., 1989, Basic Analytical Petrology, Oxford University Press, New York – Oxford, 369 p.

Rosenthal E., Adar E., Issar A.S., Batelaan O., 1990, Definition of groundwater flow patterns by environmental tracers in the multiple aquifer system of southern Arava Valley, Israel, Journal of Hydrology, vol. 117, No.1-4, p. 339-368

Salvania, N.V. and Nicholson, K., 1990, Chemometrics applied to the fluid chemistry of geothermal fields in the Taupo Volcanic Zone, New Zealand. In: Harvey, C.C., Browne, P.R.L., Freestone, D.H. and Scott, G.L. (eds.), Proceedings 12th NZ Geothermal Workshop, Auckland University, p. 157-163

Scanlon, B.R., B.K. Darling and W.F. Mullican III, 2001, Evaluation of groundwater recharge in basins of Trans-Pecos Texas, In Aquifers of West Texas. Edited by R.E. Mace, W.F. Mullican III and E.S. Angle. Austin, Texas Water Development Board Report 356, p. 26-40

Seager, W. R., 1975, Cenozoic Tectonic Evolution of the Las Cruces Area, New Mexico, New Mexico Geological Society Guidebook, 26th Field Conference, Las Cruces Country, New Mexico Geological Society, Socorro, NM, p. 241–250

Slichter, C.S., 1905, Ground Waters of Rio Grande Valley, U.S. Geological Survey, Water-Supply and Irrigation Paper No. 141, 83 p.

Sparks, D.L., 1995, Environmental Soil Chemistry, Academic Press, Inc., San Diego, 267 p.

Stewart, B.W., Capo, R.C. and Chadwick, O.A., 1998, Quantitative strontium isotope models for weathering, pedogenesis and biogeochemical cycling, Geoderma, Vol. 82, p. 173-195

Stickel, R., 1991, The effect of ground3water flow on the hydrochemical variability of groundwater in the southern Jornada Del Muerto Basin, Dona Ana and Sierra Counties, New Mexico, MS Thesis, New Mexico State University, Las Cruces, New Mexico, 111 p.

Swanberg, C.A., 1975, Detection of geothermal components in groundwaters of Dona Ana County, Southern Rio Grande Rift, New Mexico, In: Las Cruces Country, New Mexico Geological Society Guidebook, 26th Field Conference, pp 175-180

Toth J., 1999, Groundwater as a geologic agent: an overview of the causes, processes and manifestations. Hydrogeology Journal, Vol. 7, p. 1-14

United States Geological Survey (USGS), 2000, http://waterdata.usgs.gov/nwis/qwdata

Veldeman, E., Van't dack, L., Gijbels, R. and Pentcheva, E.N., 1990, Thermal waters from south Bulgaria: A multivariate approach for evaluation and interpretation of analytical data. Geothermal Research Council T4ransactions, Vol. 14, p. 1537-1543

Vuataz, F.D. and Goff, F., 1986, Isotope geochemistry of thermal and nonthermal waters in the Valles Caldera, Jemez Mountains, northern New Mexico, Journal of Geophysical Research, Vol. 91, No. B2, p. 1835-1853

Walton, J., Ohlmacher, G., Utz, D., and Kutianawala, M., 1999, Response of the Rio Grande and Shallow Ground Water in the Mesilla Bolson to Irrigation, Climate Stress, and Pumping, Environmental & Engineering Geoscience, Vol. V, No. 1, p 41-50

White, D.E., 1957, Thermal waters of volcanic origin, Bulletin of the Geological Society of America, Vol. 68, p. 1637-1658

Wilson, C.A., White, R.R., Orr, Brennon R., and Roybal, R.G., 1981, Water Resources of the Rincon and Mesilla Valleys and adjacent areas, New Mexico, New Mexico State Engineer, Technical Report 43, 514 p.

Williams, J.H., 2001, Salt balance in the Rio Grande project from San Marcial, New Mexico to Fort Quitman, Texas, MS Thesis, New Mexico State University, Las Cruces, New Mexico, p. 42

Williams R.E., 1982, Statistical identification of hydraulic connections between the surface of a mountain and internal mineralized zones, Ground Water, Vol. 20, p. 466-478

Witcher, J.C., 1981, Thermal springs of Arizona, in field notes: State of Arizona Bureau of Geology and Mineral Technology, V. 11, No. 2, p. 1-4

Witcher, J.C., King, J.P., Hawley, J.W., Kennedy, J.F., Williams, J., Cleary, M. and Bothern, L., in press, Sources of salinity in the Rio Grande and Mesilla Basin groundwater, WRRI Technical Completion Report 330, New Mexico Water Resources Research Institute, New Mexico State University, Las Cruces, New Mexico